Current Research in Neurobiology 4 (2023) 100065

Contents lists available at ScienceDirect

Current Research in Neurobiology

journal homepage: www.sciencedirect.com/journal/current-research-in-neurobiology

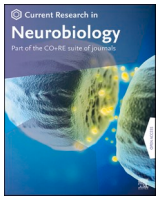

Characterisation of functional deficits induced by AAV overexpression of alpha-synuclein in rats

F. Gubinelli [a], L. Sarauskyte [a], C. Venuti [a], I. Kulacz [a], G. Cazzolla [a], M. Negrini [a], D. Anwer [a], I. Vecchio [a], F. Jakobs [a], F.P. Manfredsson [b], M. Davidsson [b,c], A. Heuer [a,*]

[a] Behavioural Neuroscience Laboratory, Department of Experimental Medical Sciences, Lund University, Lund, Sweden
[b] Department of Translational Neuroscience, Barrow Neurological Institute, Phoenix, AZ, USA
[c] Molecular Neuromodulation, Department of Experimental Medical Sciences, Lund University, Lund, Sweden

ARTICLE INFO

Keywords:
Parkinson's disease
Choice reaction time
Alpha-synuclein
AAV
Visuo-spatial neglect

ABSTRACT

Background: In the last decades different preclinical animal models of Parkinson's disease (PD) have been generated, aiming to mimic the progressive neuronal loss of midbrain dopaminergic (DA) cells as well as motor and non-motor impairment. Among all the available models, AAV-based models of human alpha-synuclein (h-aSYN) overexpression are promising tools for investigation of disease progression and therapeutic interventions.
Objectives: The goal with this work was to characterise the impairment in motor and non-motor domains following nigrostriatal overexpression of h-aSYN and correlate the behavioural deficits with histological assessment of associated pathology.
Methods: Intranigral injection of an AAV9 expressing h-aSYN was compared with untreated animals, 6-OHDA and AAV9 expressing either no transgene or GFP. The animals were assessed on a series of simple and complex behavioural tasks probing motor and non-motor domains. Post-mortem neuropathology was analysed using immunohistochemical methods.
Results: Overexpression of h-aSYN led to progressive degeneration of DA neurons of the SN and axonal terminals in the striatum (STR). We observed extensive nigral and striatal pathology, resembling that of human PD brain, as well as the development of stable progressive deficit in simple motor tasks and in non-motor domains such as deficits in motivation and lateralised neglect.
Conclusions: In the present work we characterized a rat model of PD that closely resembles human PD pathology at the histological and behavioural level. The correlation of cell loss with behavioural performance enables the selection of rats which can be used in neuroprotective or neurorestorative therapies.

1. Introduction

Cognitive decline and dementia significantly contribute to a reduction in the quality of life of patients suffering from Parkinson's disease (PD) and related disorders. Despite being major causes of disability, these symptoms do not respond well to standard treatments. Whereas the motor consequences have been heavily studied, preclinical investigations have largely neglected psychiatric and cognitive symptoms, although up to 80% of Parkinson's patients develop symptoms such as dementia. The development of preclinical rodent models that display relevant histopathological as well as behavioural features is imperative for the development and evaluation of therapeutic approaches. Traditional preclinical rodent models of PD are based on a chemically induced lesion, e.g., by 6-hydroxydopamine (6-OHDA) administration along the nigrostriatal pathway, which results in a rapid degeneration of the dopaminergic (DA) cell bodies and their striatal terminals (Ungerstedt, 1968; Kirik et al., 1998) and a unilateral injection results in behavioural impairments in motor and sensorimotor domains manifesting contralateral to the side of injection (Olsson et al., 1995; Kirik et al., 1998; Schallert et al., 2000). Despite being an excellent model for testing dopamine replacement strategies, it lacks several of the histopathological hallmarks visible in the human disease such as neuronal and axonal inclusions in the form of alpha-synuclein (aSYN) or neurofilament aggregates, termed Lewy bodies and Lewy neurites,

* Corresponding author. Behavioural Neuroscience Laboratory, Department of Experimental Medical Sciences, Lund University, Sölvegatan 19, 22 184, Lund, Sweden.
E-mail address: andreas.heuer@med.lu.se (A. Heuer).

https://doi.org/10.1016/j.crneur.2022.100065
Received 11 September 2022; Received in revised form 22 November 2022; Accepted 1 December 2022
Available online 16 December 2022
2665-945X/© 2022 The Authors. Published by Elsevier B.V. This is an open access article under the CC BY-NC-ND license (http://creativecommons.org/licenses/by-nc-nd/4.0/).

respectively (Spillantini et al., 1997). Several variations of aSYN overexpression models have been generated based on transgenic lines or viral vector-based overexpression (Kirik et al., 2002; Klein et al., 2002; Lo Bianco et al., 2002; Yamada et al., 2004; Chung et al., 2009; Magen and Chesselet, 2010; Decressac et al., 2012b; Gubinelli et al., 2022; Negrini et al., 2022). Transgenic animals do not recapitulate the severe behavioural impairments seen in the human disease, and the first generation of viral vector-based models were variable in lesion severity within an experimental group (Kirik et al., 2002; Lo Bianco et al., 2002). The level of nigrostriatal degeneration varies considerably between vector serotypes, promotor-transgene combinations, and production batches, but also within experimental groups. At present, many therapeutical approaches are preclinically tested in rodent models using simple tests of motor asymmetry, such as the stepping test, the cylinder test or the drug-induced rotation tests. However, PD is notably a much more complex disorder affecting many motor and non-motor domains. Despite the inability to recapitulate the entirety of human motor function in the rat, we can identify and probe specific features. In human PD patients it is movement initiation and sequencing of voluntary movements that is more affected than muscle strength and patients display distinctive impairments in simple and choice reaction time tasks (Rogers and Chan, 1988). Rodents with unilateral dopamine lesions develop distinct impairments in the speed and accuracy of initiating motor responses on the side of the body opposite to the lesion whilst the execution speed is impaired bilaterally (Carli et al., 1983; Robbins et al., 1983; Brasted et al., 1998; Dowd and Dunnett, 2004; Dowd et al., 2005b; Heuer and Dunnett, 2012, 2013; Heuer et al., 2013a, 2013b, 2013c). Furthermore, visual dysfunction has frequently been reported in patients with PD (Boller et al., 1984; Levin et al., 1991; Davidsdottir et al., 2005). Patients who are affected with a lateralised deficit often present with a bias towards the less affected side on several tests of visuo-spatial function (Villardita et al., 1983; Lee et al., 2001b; a; Harris et al., 2003; Laudate et al., 2013) and visual dysfunction is associated with cognitive impairment (Davidsdottir et al., 2005). We have recently characterised a novel iteration of the AAV-h-aSYN overexpression model and demonstrated the development of stable behavioural deficits on a series of commonly used motor tests as well as the development of histopathological features that closely resemble Lewy body-like structures (Gubinelli et al., 2022; Negrini et al., 2022).

The aim of the present study was twofold: Firstly, we aimed to characterise the behavioural deficits which manifest after AAV-h-aSYN overexpression on the lateralised choice reaction time task which allows for the dissociation of movement times, reaction times, as well as response accuracy towards stimuli presented ipsilateral or contralateral to the lesion. Secondly, we aimed to correlate the behavioural deficits with the degeneration and histopathology that develops in the nigrostriatal dopaminergic pathway. The lateralised choice reaction time task utilized in the present study is conducted in the 9-hole operant chamber. The animals have to execute a lateralised response to brief visual stimuli that are randomly presented to either side of the animals' head, which allows for a dissociation of movement initiation and response times to either side of the animals' body (Carli et al., 1985). The ability to characterise the precise nature of the deficit will help to guide and analyse therapeutical interventions. Behavioural readouts tap in to motor and non-motor domains such as reaction and movement times, motivation, and attentional neglect. Based on the data presented in the current manuscript we demonstrate – for the first time-the development of lateralised neglect on a choice reaction time task in rats following intranigral h-aSYN overexpression, in addition to behavioural deficits on several motor tasks. Animals with moderate lesions were identified by a combined deficit on the behavioural tasks at the earliest timepoint. Importantly, the observed deficits developed progressively and are thus useful for the selection of animals for downstream investigations into neurorestorative or neuroprotective therapies.

2. Materials and methods

2.1. Experimental outline

A schematic of the experimental timeline and the respective groups is presented in Fig. 1A. After habituation and food restriction animals were trained on the behavioural tasks outlined below. After baseline performance had been collated, rats were matched on their combined performance on all tasks into the following experimental groups: uninjected control (control), AAV no transgene (AAV-noTG), AAV GFP (AAV-GFP), AAV human wild type alpha-synuclein (AAV-h-aSYN) and 6-hydroxydopamine (6-OHDA) (Fig. 1A). After surgery (Fig. 1B and C), we monitored the development of behavioural deficits at 4-, 8- and 12-weeks post-lesion on the simple behavioural tasks and at the 12-week timepoint for 15 consecutive days on the operant task (until week 14) (Fig. 1D). After all post-lesion behavioural data have been collected and analysed, animals were perfused (week 16), and brains were extracted and collected for further analysis.

2.2. Assignment to experimental groups

Of the 36 rats that were injected with the AAV-h-aSYN vector we stratified the animals into mild and moderate impairment groups, based on their behavioural performance. As has been reported previously in a similar study correlating the behavioural deficits after unilateral 6-OHDA injections with the extent of damage to nigrostriatal DA system (Grealish et al., 2010) we assigned animals to different groups based on their combined performance on three commonly used tests of motor function. Animals that presented a bias score >20% on each of the three simple motor tasks (cylinder, stepping and corridor test) were placed in the moderate group, whereas animals that did display a bias of <20% were assigned to the mild impaired group. The final group sizes were as following: control, n = 8; AAV-noTG, n = 6; AAV-GFP, n = 12; AAV-h-aSYN mild, n = 24; and AAV-h-aSYN moderate, n = 12; 6-OHDA, n = 9.

2.3. Animals

Sprague-Dawley rats (females, 250 g on arrival, approximately 63 days old, n = 71) sourced from Janvier (France) were kept under a 12:12 h light/dark cycle, constant temperature of 21 °C, 50% humidity, and *ad libitum* access to water and food, except during periods of food restriction as outlined below. After arrival, animals were housed for 5 days for acclimatization, before starting any experimental procedure. Surgical and experimental procedures were designed, approved, and performed in accordance with the EU directive for the use of animals in research (2010/63/EU), approved by the local ethical committee and registered with the Swedish Department of Agriculture (Jordbruksverket).

2.4. AAV production

AAV9-CBA-h-aSYN (AAV-h-aSYN) and AAV9-CBA-no transgene (AAV-noTG) viruses were produced as previously described using chloroform extraction (Davidsson et al., 2020; Negrini et al., 2020). Briefly, for h-aSYN, HEK293T cells were triple transfected with ITR-transgene, pAAV2/9n and the helper plasmid pXX6 using PEI. AAVs were harvested 72h post-transfection using polyethylene glycol 8000 (PEG8000) precipitation and chloroform extraction followed by PBS exchange in concentration columns. AAV9-CBA-GFP (AAV-GFP) was produced as previously described using Iodixanol gradient ultracentrifugation (Sandoval et al., 2019; Davidsson et al., 2020). In brief, the ITR flanking genome was packaged into AAV9 capsids using PEI transient transfection. HEK293 cells were triple transfected with transgene, pAAV2/9n and the helper plasmid pXX6. AAVs were purified using an iodixanol ultracentrifugation gradient and concentrated in

A

Group	Capsid / Transgene	Description	Abbreviation
Control	-	Unlesioned	Control (n = 8)
AAV-noTG	AAV9 / -	No viral genome	noTG (n = 6)
AAV-GFP	AAV9 / GFP	Green Fluorescent Protein	GFP (n = 12)
AAV-h-aSYN	AAV9 / h-aSYN	Human Wild Type aSYN	h-aSYN (n = 36)
6-OHDA	-	Neurotoxicant	6-OHDA (n = 9)

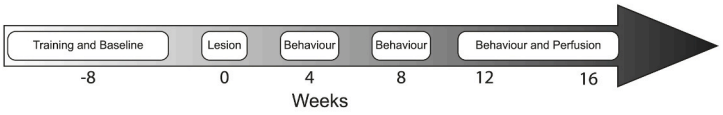

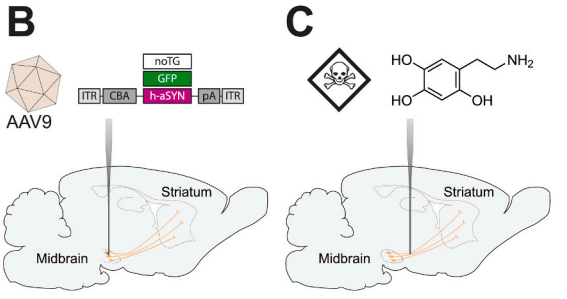

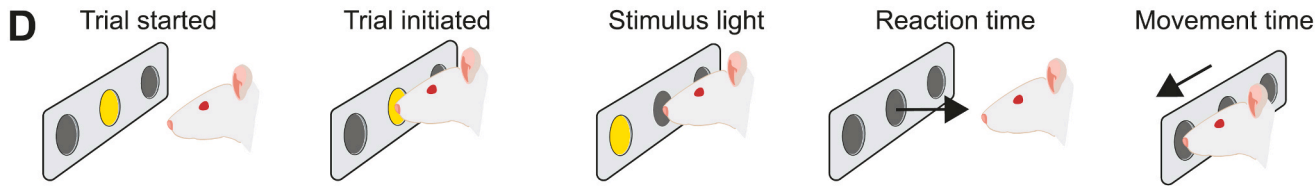

Fig. 1. Experimental outline and lateralised choice reaction time task overview.
A: Table of group descriptions and timeline of key experimental timepoints. **B:** Schematic of AAV vector capsid and transgene cassette displaying the construct used in the current experiment and the injection sites into the rat midbrain. noTG = no transgene, GFP = green fluorescent protein, h-aSYN = human alpha-synuclein, 6-OHDA = 6-hydroxydopamine, pA = polyadenylation, ITR = Inverted Terminals Repeats, CBA = Chicken Beta Actin. **C:** Schematic of 6-OHDA injection aimed at the medial forebrain bundle. **D-F:** Schematic representation of the lateralised choice reaction time task. A trial is started with an illumination of the centre hole. The rat is then required to perform a sustained nose-poke into the illuminated hole. After a variable delay a brief (300 ms) visual stimulus is presented randomly to either side of the animals' head. The rat is then required to respond with a nose-poke into the previously illuminated hole in order to obtain a food reward. The time taken from stimulus presentation to withdrawal from the centre hole is indicative of the reaction time whereas the time from withdrawal to execution of the lateralised response is taken as movement time.

concentration columns. For each production, six 500 cm^2 flasks were used, resulting in 200 μL purified AAV vector. AAVs were titered using droplet digital PCR (ddPCR)(Hindson et al., 2011; Lock et al., 2014), with primers specific for the ITRs (forward primer 5′-CGG CCT CAG TGA GCGA-3′ and reverse primer 5′-GGA ACC CCT AGT GAT GGA GTT-3′). Titers were then normalized to 2.5×10^{12} genome copies (gc)/ml using modified Phosphate Buffer Saline (PBS) Mg^{++}/Ca^{++}.

2.5. Stereotaxic surgery

Animals were anesthetised with a mixture of 5% isoflurane with oxygen as carrier gas and placed into a stereotactic frame. Injections were performed using a pulled glass capillary connected to a 10 μl Hamilton syringe (Heuer et al., 2013a). For the AAV-noTG, AAV-GFP and AAV-h-aSYN groups, 4 μl of virus (2 μl per coordinate) were unilaterally injected into the substantia nigra (SN) at two different sites (in mm from Bregma): i.) A/P: −5.3, M/L: −1.8, D/V: −8; ii.) A/P: −5.6, M/L: −2.5, D/V: −7.5. For the 6-OHDA group, a single unilateral injection of 3 μl of toxin (4 μg/μL, calculated from freebase weight HBr salt) was performed in the medial forebrain bundle (MFB) at the following coordinates (in mm from Bregma): A/P: −4.0, L: −1.3, V: −7.0 (Torres et al., 2011). All injections were performed at 0.5 μl/min and the needle was left in place for an additional 4 min to allow for diffusion, and then gently removed.

2.6. Behavioural analysis

All behavioural tests and analysis were performed by the same researcher, blinded to the respective experimental group. All the animals were placed on a food restriction regimen (85%–90% of their free-feeding body weight) one week prior to the onset of behavioural testing. We first assessed the behavioural performance on the Cylinder test and the Stepping test followed by the corridor test and the lateralised choice reaction time task at each timepoint. After the behavioural data had been collated for each time-point, animals were returned to *ad libitum* access to food.

2.6.1. Stepping

Forelimb akinesia test (stepping test) was performed as described previously (Olsson et al., 1995). In brief, one forelimb was restrained, and the test was performed on a benchtop surface over a distance of 90 cm over 5 s. The number of adjusting steps performed by the left and right front paws are recorded in forward and backward directions. Three consecutive repetitions for each paw (both forward and backward) were taken. The three trials for each paw were averaged and results are expressed as percentage bias score [(Contralateral – Ipsilateral)/(Ipsilateral + Contralateral)*100].

2.6.2. Cylinder

Cylinder test was performed as described previously (Schallert et al., 2000), with a trial duration of 5 min and a glass cylinder with an inner diameter of 22 cm. A total count of the first 20 touches on the cylinder's wall by the right or left forepaw were counted. Results are expressed as percentage bias score [(Contralateral – Ipsilateral)/(Ipsilateral + Contralateral)*100].

2.6.3. Corridor

The *Corridor test* was performed using the adjacent version configuration and as described previously (Dowd et al., 2005a). The corridor was fitted with 10 pairs of parallel fitted plastic wells, which were baited with five 20 mg precision sucrose pellets each. Animals were habituated for 5 min in an empty corridor, and then transferred to the testing corridor containing 20 total pots (10 adjacent). A retrieval is counted when the animal explored with the nose into the wells; the total number of 20 retrievals (or 5 min have elapsed) on the left and right sides of its body axis were counted. Results are then averaged expressed as a percentage bias score [(Contralateral – Ipsilateral)/(Ipsilateral + Contralateral)*100].

2.6.4. Lateralised choice reaction time task

Lateralised choice reaction time task was performed as previously described in detail (Dowd and Dunnett, 2004, 2005b; a; Heuer and Dunnett, 2012, 2013). Testing was performed on a bank of 9-hole operant chambers controlled by MED-PC IV software (Med Associates Inc –

USA), installed on a Windows computer. Rats were tested in daily 30-min sessions. Initial training to perform the operant task was done as reported previously (Dowd and Dunnett, 2005a; Heuer et al., 2013a). The 9-hole operant chamber is designed with a curved array of 9 response holes on one wall and a magazine connected to a pellet dispenser on the opposite wall. Furthermore, stimulus lights are installed in each of the response holes and the magazine as well as a house light. Nose-pokes into each of the response holes and the magazine are detected by infrared beams. In the operant choice reaction time task used in the present study, the centre hole (H5) as well as one hole to the left (H3) and one hole to the right (H7) with respect to the animals' head were used, whilst all other response locations were covered by well blanks. Each trial started with illumination of H5 and the rats were required to perform a sustained nose-poke into the illuminated centre hole. After a variable delay (50 ms, 100 ms, 150 ms, or 200 ms) the centre hole light was extinguished and randomly one of the two lateral response holes (H3 or H7) were briefly illuminated (300 ms). A response into the illuminated response location would result in the illumination of the magazine as well as the delivery of one reward sucrose pellet (45 mg, Sandown Scientific). An incorrect response would result in a time out interval (TOI) of 5 s with all lights extinguished. Premature withdrawals, a failure to execute the lateralised response within 3 s or repeated H5 pokes would also result in a TOI. The main outcome measures that were recorded were: total number of trials initiated (TTI), efficiency defined as total trials usable (where a lateralised response had been made)/TTI as %, accuracy (correct trials/trials usable as %), reaction time (latency from onset of the lateralised stimulus to detection of withdrawal from H5, and movement time (latency from H5 withdrawal to execution of the lateralised response) (Fig. 1D). Baseline was acquired over a period of 5 consecutive days. For the 12-weeks post lesion testing, the animals were tested over a period of 15 consecutive days with the same 300 ms stimulus-duration. As commonly done for this type of assessment, consecutive days of testing were grouped into blocks to properly assess and demonstrate the stability of the lesion (Dunnett and Iversen, 1981; Dunnett, 1985; Montoya et al., 1990; Reading et al., 1991; Brasted et al., 1997; Dunnett et al., 1999; Eagle et al., 1999; Heuer & Dunnett, 2012, 2013; Kaindlstorfer et al., 2012; Heuer et al., 2013a, 2013b, 2013c). In this study, the post-lesion testing was grouped into three blocks of 5-day each, named LX-1, LX-2, and LX-3, respectively.

2.7. Perfusion and tissues processing

Animals were sacrificed with an intraperitoneal injection of sodium pentobarbital (200 mg/kg). They were then transcardially perfused with 50 ml 0.9% saline solution, followed by 250 ml of 4% paraformaldehyde (PFA) in phosphate buffered saline (PBS) solution (pH = 7.4). Brains were extracted and post-fixed in PFA for 24h at 4 °C, and then transferred into 25% sucrose until saturated. All brains were sectioned into 40 μm coronal 1:12 series using a freezing sledge microtome (SM200R, Leica) and stored in antifreeze solution at −20 °C until use.

2.8. Proteinase K treatment

Sections were removed from the antifreeze solution and washed 3 times in PBS and then mounted on permafrost-glass. Glass slides were left to dry overnight and incubated the following day in proteinase K (pK) solution (25 μg/ml; QIAGEN) for 1 h at room temperature before proceeding with the immunostaining for human synuclein ($aSYN^{211}$) as described below.

2.9. Immunohistochemistry

All primary and secondary anti-bodies used in in the current manuscript are presented in Supplementary Table 1. DAB- and fluorescent-immunohistochemistry (DAB-IHC and FL-IHC) were performed as described previously (Heuer et al., 2013a). Briefly, sections were removed from the antifreeze solution and washed 3 times in PBS (pH = 7.4). Subsequently, sections were incubated for 15 min in PBS with 3% H_2O_2 and 10% methanol to quench endogenous peroxidase activity. Sections were then washed 3 times in PBS and incubated for 1 h at room temperature (RT) in a blocking solution (5% appropriate serum and PBS-T (PBS containing 0.25% Triton X-100)). After, sections were transferred into the primary antibody (See Supplementary Table 1) in 5% serum and incubated overnight at 4 °C with gentle agitation. The following day, sections were washed 3 times in PBS and incubated for 1 h at RT in blocking solution. Next, sections were incubated in the appropriate secondary antibody in 5% serum for 1 h at RT. Sections were then washed 3 times in PBS and incubated for 1 h with the ABC complex (ABC, Vector Laboratories) following the vendor's protocol. Sections were washed 3 times in PBS and the colour reaction was produced by incubation in DAB substrate (DAB, Vector Laboratories) with H_2O_2. After colour reaction occurred, sections were washed in PBS and mounted on gelatine-coated glass slides, airdried overnight, and then dehydrated for 5 min in increasing series of ethanol (2 × 70%, 2 × 95%, 2 × 99.5%) and lipids were removed through 2 x 5-min incubation in Xylene before cover-slipping with DPX mounting medium (Sigma). For fluorescent-immunohistochemistry, quenching, ABC, and DAB steps were omitted. Secondary antibody incubation was performed with appropriate fluorophore-conjugated antibodies, and after washing sections were either incubated for 5 min at room temperature with DAPI and then washed and mounted, or directly mounted on gelatine-coated glass slides and cover slipped once dry with PVA/DABCO mounting medium. The thioflavin S (ThioS) assay was performed as described previously (Cresto et al., 2021). Briefly, ThioS (Sigma) was diluted in 1% distilled water, filtered before each use, and kept in dark at 4 °C. After final washes, FL-IHC sections were mounted on gelatine coated slides and left to dry for few minutes. Mounted sections were then dipped in 70% and 80% ethanol for 1 min each, and then incubated for 7 min in ThioS in dark. Slides were washed for 1 min in 80% and 70% ethanol and in distilled water for 30 s before being cover slipped with PVA/-DABCO mounting medium. For DAB-immunohistochemistry, acquisition was carried out using a Leica DMI8 inverted microscope with a 20x and 63x objective. For high magnification brightfield images an Olympus A×70 microscope with a 100x objective was used. For fluorescent-immunohistochemistry acquisition was carried out using a Leica SP8 confocal microscopy using 20x and 63x objectives.

2.10. Densitometry

Scans of mounted sections were acquired using a flatbed scanner (Epson V850 Pro) at 600 DPI. The level of staining intensity was measured from 3 different consecutive striatal sections (starting point A/P: 1.6 mm) and 3 consecutive midbrain sections (starting point A/P: −4.8) for TH-DAB, aSYN-DAB using ImageJ (NIH, V.2.1.0) software. Striatal boundaries between dorsal and ventral part were drawn as described elsewhere (Grealish et al., 2010). Each image was first transformed to grayscale 8-bit image and calibrated using a step-tablet from Epson with known optical density (OD) values using the Fiji Rodbard function. The area of interest was outlined, and the average grey pixel intensity value was measured. The O.D. value of the corpus callosum was used as a reference value of non-specific background and this value was subtracted from values obtained from areas of interest.

2.11. Axonal swellings quantification

TH^+ and h-$aSYN^+$ axonal swellings were quantified following TH and h-aSYN DAB-IHC in the pre-frontal cortex (PFC) and striatum (STR), respectively. For PFC, a 63x a single field of view was captured in the dorso-medial area. For the STR, three 63x fields of view were captured respectively in the dorso-medial, dorso-lateral, and central region as previously described (Decressac et al., 2012b; Phan et al., 2017). Z-stack images for each area were acquired using a Leica DMI8 inverted

microscope with a z-step size of 1 μm though the entire thickness of the tissue. Images were then 3D stacked together using Fiji software and the number of TH^+ and h-aSYN$^+$ axonal swellings were quantified as described previously (Quintino et al., 2022). Swellings were defined as 3D immunoreactive structures with a volume larger than 3 μm^3 (Decressac et al., 2012b) and a circularity of 0.3–1 (Phan et al., 2017). Results were expressed as total number of TH^+ and h-aSYN $^+$ swellings with a volume larger than 20 μm^3.

2.12. Cell quantification

2.12.1. Stereology

Quantifications of TH-DAB-positive cells was performed according to previously published protocol (Ip et al., 2017) for unbiased stereology. Briefly, standardized z-stack mosaic images of 8–11 midbrain-stained sections with a spacing of 240 μm were acquired with a 20x magnification using a Leica bright field microscopy. Files were then stacked together using Fiji software, and TH^+ cells were counted in the areas of interest (SN) using the protocol with following changes: *a)* grid size: 170 μm × 170 μm, *b)* optical dissector size: 20 μm, *c)* length of one side optical dissector 55 μm. Only cells inside the areas of interest and following the rules valid for unbiased stereology were counted. Results are expressed as percentage of loss (%) to the contralateral hemisphere.

2.12.2. NeuN count

NeuN$^+$ cells were quantified manually in the ipsilateral and contralateral SN as described previously (Negrini et al., 2022). In brief, z-stacks of 1 μm through the entire thickness of the tissue (40 μm) were taken with a Leica DMI8 microscope at ×20 magnification. Individual image stacks were mosaic merged to generate one overview image of the entire midbrain at the level A/P: −5.0 mm from Bregma. We utilized the medial terminal nucleus of the accessory nucleus of the optic tract as a visual landmark to delineate the VTA and the SN. The final images were uploaded into ImageJ and the cell counter plugin was used to count individual cells in the SN by an experimenter blinded with regards to experimental groups.

2.12.3. Microglial count

Microglial cells were quantified using an in house developed AI-based algorithm for images detection following IBA1 DAB-IHC in the SN. For AI training, IBA1 z-stack images of different midbrain areas were acquired in RGB using a Leica DMi8 inverted microscope with a z-step size of 1 μm though the entire thickness of the tissue. Images were processed to EDF and were divided into training, validation, and a test dataset with 600, 120, and 120 images, respectively. Bounding boxes were manually created using the roboflow online annotation tools and exported to *coco* format for the training model. The final training set contained a total of 15249 cells and an average of 22.4 cells per image. The architecture of the Faster RCNN model with the backbone ResNet-101 were trained on the training dataset and evaluated on the test dataset using detectron2 vision library implemented in PyTorch. Faster RCNN (Ren et al., 2017) is a two stage architecture containing a region proposal network, that generates region proposals, which is concurrently fed to the detector network for object classification. The loss function of Faster RCNN consists of a classification loss function to penalize incorrect classification and the bounding box loss function to compute the mean absolute difference between the true and the predicted bounding boxes. For training, SGD solver were used with base learning rate 0.001, LR scheduled with gamma of 0.05 and a keeping batch size 4. The model was trained on Google Colab pro for 100 epochs. For evaluation of the model, the mean average precision was taken into consideration. Mean average precision is the mean of average precision over all categories and intersection of union thresholds. Cells were counted manually and compared with the artificial neural network approach by calculating the Pearson correlation coefficient between them. Final quantifications were then performed on three 20x images of the SN of the injected and non-injected side for each animal. Images were taken as z-stacks using a Leica DMI8 inverted microscope with a z-step size of 1 μm though the entire thickness of the tissue. Results are expressed as average number of IBA1+ cells in the ipsilateral and contralateral side of each group.

2.13. Quantitative real-time PCR (qPCR)

To assess the degree of nigral h-aSYN overexpression, the SN was dissected from PFA-fixed sections. Briefly, 3 sections of the central midbrain were washed 3x in sterile DPBS (Gibco), and then the SN of the injected hemisphere was dissected with sterile blade. The tissue was homogenised, and RNA was extracted using RNA extraction kit for fixed tissues (E.Z.N.A. FFPE RNA Kit, Omega Bio-Tek) following the vendor's protocol. The RNA concentration was determined using a NanoDrop (Thermo Scientific). Reverse transcription was performed with 300 ng of RNA following vendor's protocol (iScript cDNA Synthesis Kit – Biorad). SYBR green qPCR was performed using iTaq Universal SYBR Green Supermix (Biorad), following standard procedures and in triplicates. The data were quantified using the ΔCt-method and normalized to GAPDH. GAPDH and h-aSYN primer (specific to human aSYN) sequences were previously validated and published (Aldrin-Kirk et al., 2014): GAPDH: fwd 5′-CAA CTC CCT CAA GAT TGT CAG CAA-3′, rev 5′-GGC ATG GAC TGT GGT CAT GA-3'; h-aSYN: fwd 5′-CAG GGA GCA TTG CAG CA-3′, rev 5′-GTG GGG CTC CTT CTT CAT TC-3'.

2.14. Statistics

Data (excluding operant behavioural data) were analysed using GraphPad Prism V.8 with a significance level of $\alpha = 0.05$ for all the analysis. For multigroup comparison, one-way ANOVA followed by Bonferroni *post-hoc* test was used. When two variables were present, repeated measures ANOVAs with Tukey's *post-hoc* test was used (group and weeks as dependant variables). Levels of significance in the figures were showed in comparison to the control group. For pairwise and non-pairwise comparisons respectively paired or unpaired Students *t*-test was applied. All operant behavioural data were analysed using GENSTAT v13.1 software package with Newman-Keuls post hoc test for multiple comparisons. A significance level of $\alpha = 0.05$ was chosen for all analyses. The operant behavioural data were analysed using a repeated measures analysis of variance with the factors Group (control, noTG, GFP, h-aSYN mild, h-aSYN moderate, 6-OHDA), Week (Baseline, LX-1, LX- 2, L-3), and Side (Ipsilateral, Contralateral). All data were collated over a 5-day block of testing and response latencies (reaction and movement times) are expressed as arithmetic mean ± SEM. The main outcome measures analysed were the number of usable trials (Total trials usable, TTU), Efficiency (Total trials initiated/TTU*100), Accuracy (Correct trials/TTU*100), Latencies for correct responses (Correct reaction time, CRT and correct movement time, CMT). TTU and Efficiency are summed over the 4 delays whereas the remaining parameters were averaged over the 4 delays. For correlation analysis we used linear (r coefficient of Spearman) regressions with a significance level set at $\alpha = 0.05$. Levels of significance annotations are as following: *$p < 0.05$; **$p < 0.01$; ***$p < 0.001$ and are only presented for significant differences with the control group. The full table of all cross comparisons made for all behavioural tests are provided in tabular form in Supplementary Tables 2–12. All data were expressed with SEM error bars.

2.15. Data sharing

All materials and data will be made available upon reasonable request.

3. Results

Recently we characterised a novel iteration on the AAV-vector based

overexpression model using h-aSYN to model early (Gubinelli et al., 2022) and advanced (Negrini et al., 2022) parkinsonism in rats. In these studies, we observed classic anatomopathological nigrostriatal degeneration, as well as progressive appearance of behavioural deficits, depending on the severity of the nigrostriatal degeneration. The aim of the present study was to evaluate and characterise impairment in the motor and non-motor domains arising after unilateral intranigral AAV-h-aSYN overexpression in rats on a complex motor learning task. We aimed to correlate the behavioural deficits with the degeneration and histopathology that develops in the nigrostriatal dopaminergic pathway following h-aSYN overexpression and to establish criteria that would indicate whether the behavioural deficits were stable. Therefore, we allocated rats of the h-aSYN group into a mild and a moderate lesion group, based on their behavioural impairments on a combined deficit of >20% on three tests of motor behaviour, as previously reported in mice (Grealish et al., 2010).

3.1. Overexpression of h-aSYN leads to a stable protein expression in striatum and midbrain

We first evaluated the level of transgene expression following AAV delivery at 16 weeks post injection for the AAV-GFP, AAV-h-aSYN mild and AAV-h-aSYN moderate group. DAB-IHC for GFP and human h-aSYN revealed strong expression of either GFP or h-aSYN in striatal terminals and nigral cell bodies in the ipsilateral hemisphere for all the respective groups (Fig. 2A–C). O.D. analysis of high magnification images of transgene expression in the striatum (STR) (Fig. 2D and E and 2H-J) revealed a significant difference between the ipsilateral and contralateral hemispheres in animals of the AAV-GFP ($t_{11} = 5.17$, $p < 0.001$), AAV-h-aSYN mild ($t_{23} = 12.76$, $p < 0.001$) and AAV-h-aSYN moderate group ($t_{11} = 9.49$, $p < 0.001$). Similarly, O.D. analysis of high magnification images from midbrain sections (Fig. 2F and G and 2K-M) revealed a significant difference between the ipsilateral and contralateral injected substantia nigra (SN) for the AAV-GFP ($t_{11} = 4.90$, $p < 0.001$), AAV-h-aSYN mild ($t_{23} = 15.12$, $p < 0.001$) and AAV-h-aSYN moderate group ($t_{11} = 9.47$, $p < 0.001$). This suggests that the transgene expression was similar in all AAV injected groups. No h-aSYN or GFP labelling could be detected in animals of the untreated control or the 6-OHDA group (data not shown). To confirm overexpression and localization of h-aSYN in the AAV-h-aSYN moderate SN, we performed qPCR specifically against overexpressed h-aSYN (Supplementary Fig. 1A) which demonstrated strong h-aSYN transgene overexpression (Group; $F_{2,15} = 10.34$ $p < 0.01$) when compared with the control and AAV-noTG group (both, $p < 0.01$). To further confirm the expression of the transgenes of interest (h-aSYN and GFP) in midbrain dopaminergic cells, we performed fluorescent immunohistochemical (FL-IHC) labelling for GFP or h-aSYN ($aSYN^{211}$), tyrosine-hydroxylase (TH) and the Vesicular Monoamine Transporter 2 (VMAT2) (Fig. 2N-O_{III}). As can be seen from the high magnification images, the transgenes of interest were strongly expressed in dopaminergic cells. Furthermore, we observed that overexpression of h-aSYN led to the formation of phosphorylated synuclein ($pSer^{129}$), a classic histopathological hallmark of human Lewy bodies (Fig. 2P-P_{III}).

3.2. Overexpression of h-aSYN leads to neurodegeneration of the nigrostriatal dopaminergic system

After confirming overexpression of GFP and h-aSYN in midbrain dopamine (DA) neurons, we investigated whether the presence of h-aSYN would induce physiological changes in the nigrostriatal DA system. Using tyrosine-hydroxylase (TH) as a marker for DA cells and fibres, we performed DAB-IHC labelling for TH for all groups. The transgene overexpression (GFP or h-aSYN) as well as the injection of 6-OHDA lead to degeneration of DA fibres and cell bodies along the nigrostriatal pathway ipsilateral to the side of injection (Fig. 3A–D; Supplementary Figs. 2A–B). High magnification images of coronal striatal (Fig. 3E–J) and nigral (Fig. 3E_I-J_I) sections labelled for TH also revealed a reduction in the striatal axonal density, as well as in nigral cell bodies and fibres for the GFP, h-aSYN (both mild and moderate) and 6-OHDA; this was not visible in the control and noTG groups.

Quantification of staining intensity using optical density (Fig. 3K) revealed no reduction in TH immunoreactivity in striatal sections for the control group ($t_7 = 1.15$, p = n.s.) and the noTG group ($t_5 = 0.75$, p = n.s.), whereas a significant reduction was detected in the h-aSYN mild ($t_{23} = 6.75$, $p < 0.001$), h-aSYN moderate ($t_{11} = 5.24$, $p < 0.001$), GFP ($t_{11} = 2.33$, $p < 0.05$) and 6-OHDA groups ($t_8 = 16.08$, $p < 0.001$). Subsequently we performed unbiased stereological quantification at 16 weeks post lesion (Fig. 3L) to quantify the cellular loss of TH-labelled cells in the SN. There was a significant difference between the experimental groups (Group; $F_{5,63} = 51.65$, $p < 0.001$) in the percentage of TH cell loss on the injected side. There was no bias in the number of TH^+ cells between the ipsilateral and contralateral SN in animals of the control (0.7%) and noTG (4%) (both, p = n.s.). Cell loss was highest in the animals injected with the neurotoxin 6-OHDA (85%), GFP (44%) and h-aSYN moderate (27%) groups (all vs control, $p < 0.001$). Although animals of the mild group did display a TH cell loss of 15%, this was not significantly different from the control group.

To confirm that the neurons are lost, rather than a loss of the TH phenotype, we also quantified the total number of neurons using the pan neuronal maker NeuN (Fig. 3M) and FL-IHC co-labelling for TH and NeuN (Supplementary Figs. 2C–H) for all experimental groups. In line with our previously published results (Gubinelli et al., 2022; Negrini et al., 2022), the loss of TH coincides with a loss of $NeuN^+$ cells in the SN (Group; $F_{5,49} = 4.60$, $p < 0.01$), in the transgene overexpression groups and the 6-OHDA group, confirming the degeneration of dopaminergic cells. Interestingly, whereas the loss of $TH^+/NeuN^+$ cells was limited to the location of the A9 cell group in the 6-OHDA group (Supplementary Fig. 2H), in groups where a transgene was overexpressed this loss extended to surrounding nuclei (Supplementary Figs. 2E–G). This suggests that the overexpression of the transgenes leads to a degeneration and loss of dopaminergic cells in the ipsilateral SN.

3.3. Behavioural evaluation on simple and complex behavioural tasks

3.3.1. Simple behaviour

We evaluated the development of motor deficits on a series of simple behavioural tests that are well established for unilateral dopaminergic lesions using the neurotoxicant 6-OHDA or the AAV vector-based overexpression of h-aSYN (Olsson et al., 1995; Schallert et al., 2000; Dowd et al., 2005a; Gubinelli et al., 2022; Negrini et al., 2022). Behavioural performance was assessed using the cylinder and stepping test at baseline, 4- and 8-weeks and on the corridor test at baseline, 8- and 12 weeks post-surgery.

3.3.1.1. Cylinder test. Forelimb use asymmetry was assessed using the Cylinder test. There was a significant difference in forelimb use asymmetry between the experimental groups at the 3 timepoints (Fig. 4A; Week*Group, $F_{10,121} = 9.62$; $p < 0.001$). Post-hoc analysis revealed a significant difference in the percentage bias of the 6-OHDA lesion group (79%) at the 4-week timepoint, compared to all experimental groups (control: 1%, noTG: 13%, GFP: 17%, and h-aSYN mild: 15%; all, $p < 0.05$) with exception of the h-aSYN moderate group (p = n.s.). Interestingly, although the animals of the h-aSYN moderate group displayed a reduced use of the contralateral paw (44%), this failed to reach significance at this timepoint. At the 8-week time-point, the 6-OHDA lesioned group bias remained stable (81%). Interestingly the h-aSYN moderate group bias increased at the 8-week time-point (70%) which was significantly different to the control and noTG (both, $p < 0.001$) and the GFP group (30%; $p < 0.05$). This is indicative of a progressively developing bias which manifests at similar levels to the one of a classical neurotoxin lesion, albeit over a longer duration. Animals of the h-aSYN

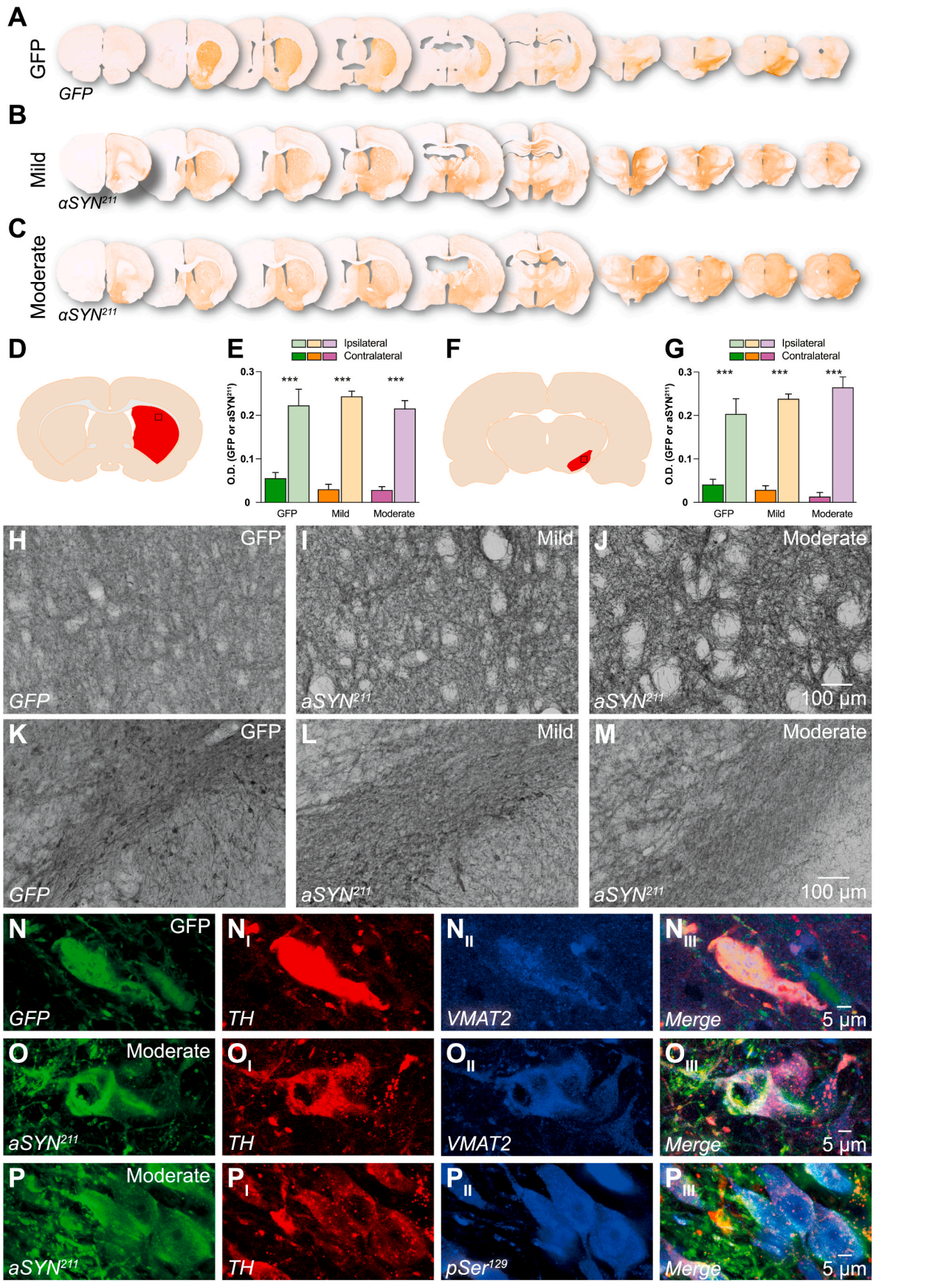

(caption on next page)

Fig. 2. Evaluation of transgene overexpression.
A-C: Representative overviews for the GFP (A), h-aSYN mild (B) and h-aSYN moderate (C) labelled for GFP and aSYN^{211}, respectively. **D:** Schematic representation of the analysed area for striatal optical density. Red area represents the striatum, while the black square represents the area where microscope picture was acquired. **E:** Optical Density measurements comparing GFP and aSYN^{211} labelling intensity between the ipsilateral and contralateral striatum. Data are expressed as mean ± SEM; *** = $p < 0.001$. **F:** Schematic representation of the analysed area for midbrain optical density. Red area represents the substantia nigra, while the black square represents the area where microscope picture was acquired. **G:** Optical Density measurements comparing GFP and aSYN^{211} labelling intensity between the ipsilateral and contralateral substantia nigra. Data are expressed as mean ± SEM; *** = $p < 0.001$. **H-J:** Representative brightfield photomicrographs of striatal sections labelled for GFP (H) and h-aSYN (I–J) respectively for the GFP and h-aSYN mild and moderate groups. **K-M:** Representative brightfield photomicrographs of midbrain sections labelled for GFP (K) and aSYN^{211} (L–M) respectively for the GFP and h-aSYN mild and moderate groups. **N–N$_{III}$:** High magnification confocal microscope images of individual neurons in the midbrain of the AAV-GFP injected group demonstrating colocalization between GFP, TH and VMAT2. **O-P$_{III}$:** High magnification confocal microscope images of individual neurons of the h-aSYN moderate group demonstrating a colocalization between h-aSYN, TH and VMAT2 or pSer^{129}.

mild group did not display any deficits on the cylinder test at any of the timepoints assessed. The cylinder bias correlated significantly with TH$^+$ loss (Spearman's Rho: −0.665, $p < 0.001$) which indicates a strong relationship between the two factors (Rea and Parker, 2014) (Fig. 4I).

3.3.1.2. Stepping test. Forelimb akinesia was assessed using the stepping test (Olsson et al., 1995; Schallert et al., 2000). There was a significant bias on the stepping test between the experimental groups on the 3 timepoints assessed (Fig. 4B; Week*Groups; $F_{10,126} = 6.91$, $p < 0.001$). At the 4-weeks timepoint, animals of the 6-OHDA lesion group displayed a large bias (65%) compared to all other experimental groups (all, $p < 0.05$) whereas the h-aSYN moderate group displayed a bias of 37%, which was different from the control and the noTG groups (both, $p < 0.05$). At the 8-week timepoint the deficit of the 6-OHDA lesioned group remained stable (74%), which was significantly different from all groups (all, $p < 0.05$), except for the h-aSYN moderate group. Furthermore, the bias of animals in the h-aSYN moderate group increased and animals of this group performed significantly worse compared to all remaining groups (all, $p < 0.05$), again indicating a progressively developing deficit which reached the level of a 6-OHDA lesion over a protracted timeframe. Interestingly the h-aSYN mild group did display a significant difference (36%) from the control group ($p < 0.01$), however not from the noTG and GFP groups (both, p = n.s.). The stepping bias correlated significantly with TH$^+$ cell loss (Spearman's Rho: −0.473, $p < 0.001$) which indicates a relatively strong relationship between the two factors (Rea and Parker, 2014) (Fig. 4J).

3.3.1.3. Corridor test. Lateralised sensory-motor neglect was evaluated using the corridor test. There was a significant difference on the corridor test between the experimental groups and on the three time-points assessed (Fig. 4C; Week*Groups; $F_{10,126} = 4.38$ $p < 0.001$). Overall, the variation within groups was larger on the corridor test compared to the cylinder and stepping test, and statistical analysis revealed fewer intergroup differences. At the 8-week timepoint animals of the control, noTG, and GFP groups displayed a minor bias (12–26%), whereas the bias of the remaining groups was 34% for h-aSYN mild, 51% for the h-aSYN moderate, and 53% for the 6-OHDA group. Statistically, the there was no difference between the h-aSYN moderate and 6-OHDA groups (p = n.s.), however both groups were significantly more impaired when compared to the control (both, $p < 0.05$). At the final time-point of assessment, again, only the h-aSYN moderate (81%) and the 6-OHDA (90%) groups displayed a bias which was significantly different from the control, the GFP and the h-aSYN mild groups (all, $p < 0.05$). The corridor bias correlated significantly with TH$^+$ loss (Rho: −0.410, $p < 0.001$) which indicates a relatively strong relationship between the two factors (Rea and Parker, 2014) (Fig. 4K).

In summary these results reveal a stable deficit on all three behavioural tests in the 6-OHDA lesion group which was detectable at the earliest timepoints assessed. The performance on all three behavioural tests correlated highly with the TH cell loss seen in the midbrain. In the h-aSYN overexpression model, the behavioural deficits developed progressively over time in animals of the h-aSYN moderate group and was similar to the 6-OHDA deficit at the final behavioural timepoint. The progressive nature of the deficit over the protracted time-period will make this model relevant for testing of disease modifying targets.

3.3.2. Lateralised choice reaction time task

After confirming that rats injected with AAV-h-aSYN displayed a bias on the test of simple motor behaviour we re-tested all animals in the operant boxes on the lateralised choice reaction time task for 15 consecutive days.

3.3.2.1. Total trials usable (TTU). All rats were trained in the lateralised choice reaction time task over a 6-week period and performed at high levels during the 5-day block of data acquisition (Fig. 4D). There was no difference in the number of usable trials (TTU, 157.73 ± 10.76) between the groups on the operant task during baseline performance, indicating well matched groups (Group, $F_{5,63} = 0.63$, p = n.s.). After the surgical session, when first reintroduced into the operant boxes, all groups performed fewer TTU compared to the baseline condition (Week*Group, $F_{15,189} = 4.10$, $p < 0.001$). Post-hoc testing revealed that at the first block of retesting (LX-1) there were no differences between the control (95.78), noTG (101.57) and the GFP (111.71) groups (all, p = n.s.) and neither between the lesioned groups 6-OHDA (45.42), h-aSYN mild (69.47), and h-aSYN moderate (50.17) groups (all, p = n.s.). However, the latter three groups were performing significantly less TTU compared to the former three (all, $p < 0.05$). The control, noTG, and GFP groups did increase the number of TTU over the next two 5-day blocks (120–140 TTU on average) and at neither the LX-2 nor the LX-3 block displayed a significant difference between them (all, p = n.s.). Animals of the 6-OHDA lesion group and the moderate h-aSYN group continued to produce significantly fewer TTU than the three control groups (all, $p < 0.001$); moreover, at the latest timepoint (LX-3), they were also performing significantly fewer TTU than the h-aSYN mild group (both, $p < 0.05$).

3.3.2.2. Efficiency (EFF). Efficiency was defined as the total number of usable trials divided by the number of initiated trials expressed as a percentage. Pre-surgery, all rats performed on the operant task with a high efficiency (>90%), indicating that most of the initiated trials were completed with a lateralised response (Fig. 4E). For the first block after the surgery (LX-1), the three control groups (control, noTG, GFP) displayed a reduced efficiency, but they recovered to pre-surgery levels at block LX-2 and LX-3. Animals that received either the AAV-h-aSYN vector in the SN or 6-OHDA into the MFB became less efficient in completing the lateralised response (Week*Group, $F_{15,189} = 2.99$, $p < 0.001$). During the first block of re-testing, efficiency was 59% for the h-aSYN mild, 47% for the h-aSYN moderate and 55% for the 6-OHDA group; this was significantly lower than the EFF observed for three control groups (all, $p < 0.01$). These groups also increased their EFF over the next two blocks of testing (LX-2 and LX-3) with the h-aSYN mild group (84%) not performing significantly different from the three control groups (all, p = n.s.); on the other hand, the h-aSYN moderate (74%) and 6-OHDA (69%) groups performed with significantly lower EFF than the three control groups (all, $p < 0.001$). This demonstrates that although animals initiated fewer trials, most of these trials were successfully completed.

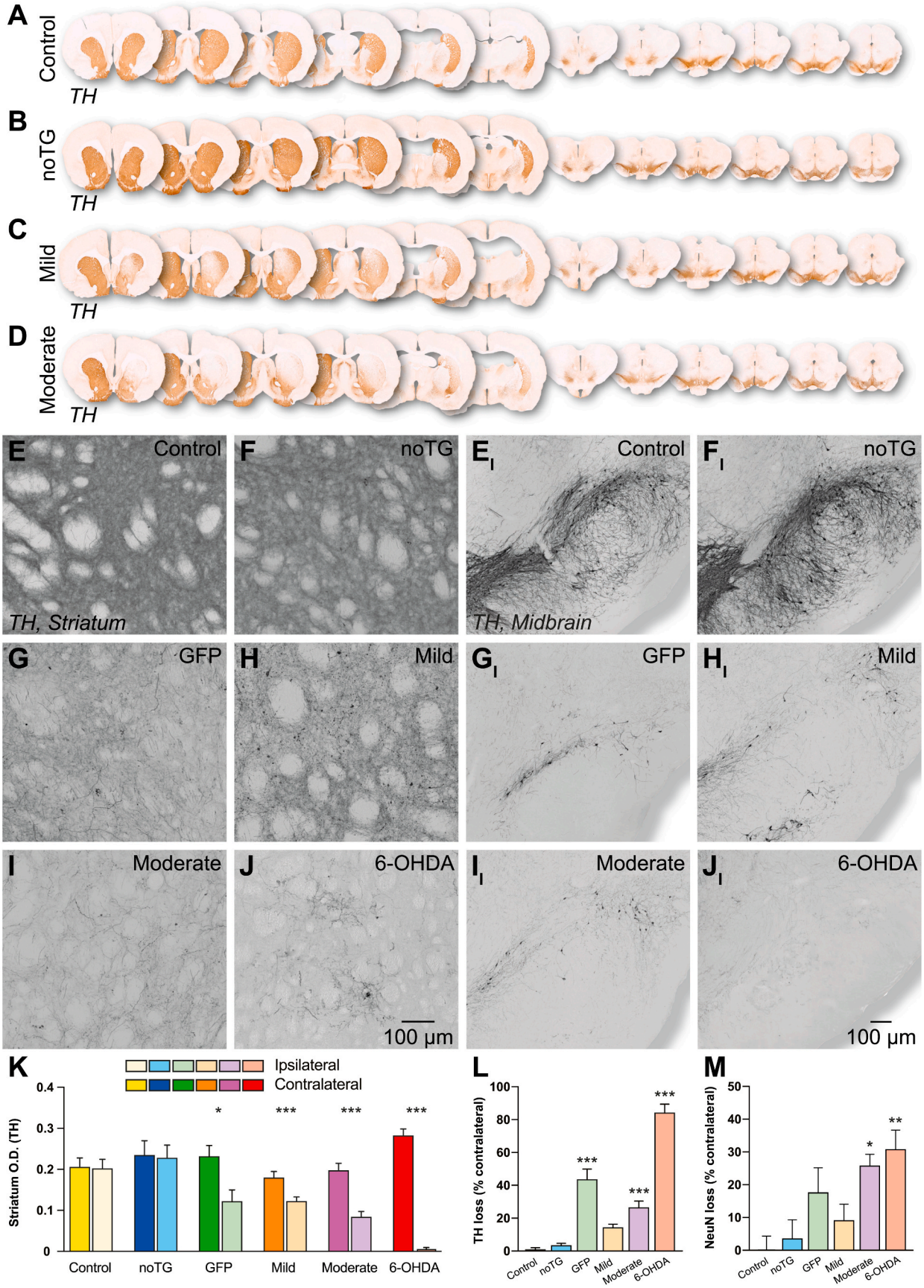

(caption on next page)

Fig. 3. Neuronal loss following AAV delivery at 16 weeks post injection.
A-D: Representative overviews of TH immunolabelling for the control group (A), noTG group (B), h-aSYN mild group (C) and h-aSYN moderate group (D). **E-J:** Representative brightfield photomicrographs of striatal sections labelled for TH for the control (E), noTG (F), GFP (G), h-aSYN mild (H), h-aSYN moderate (I), and 6-OHDA (J) groups. **E_I-J_I:** Representative brightfield photomicrographs of midbrain sections labelled for TH for the control (E_I), noTG (F_I), GFP (G_I), h-aSYN mild (H_I), h-aSYN moderate (I_I) and 6-OHDA (J_I) groups. **K:** Optical Density measurements comparing TH labelling intensity between the ipsilateral and contralateral striatum of all experimental groups. Data are expressed as mean ± SEM; * = $p < 0.05$, *** = $p < 0.001$. **L:** Percent TH cell loss quantified via unbiased stereology. Data are expressed as mean ± SEM; *** = $p < 0.001$. Significance in the figure is only displayed in relation to the control group. **M.** Percent NeuN cell loss. Data are expressed as mean ± SEM; * = $p < 0.05$; ** = $p < 0.01$. Significance in the figure is only displayed in relation to the control group.

3.3.2.3. Accuracy (ACC). During baseline testing all rats performed with a high accuracy score (>83%) in response to stimuli on both sides, which was similar for all groups (Side*Group, $F_{5,63} = 1.57$, p = n.s.) (Fig. 4F-F_I). After the surgery, rats of all groups maintained a high response accuracy when the response was directed to the ipsilateral side of the animals' head. We could already detect a significant difference between groups during baseline testing (analysis restricted to ipsilateral side; Group, $F_{5,63} = 7.51$, $p < 0.001$) where animals of the GFP and 6-OHDA group performed with higher accuracy to ipsilateral stimuli (92% and 94% respectively) when compared with the h-aSYN moderate group (both $p < 0.01$). The 6-OHDA lesioned group displayed the highest response accuracy during baseline which was also higher than the one observed for the noTG and h-aSYN moderate groups (both, $p < 0.05$). Importantly, the increased performance of the 6-OHDA lesion group is biased against our experimental hypothesis, and the h-aSYN groups did not differ significantly in their response performance from animals in the control and noTG groups. There was a small reduction in response accuracy to ipsilateral stimuli from the baseline to the first week of post-surgery testing (analysis restricted to ipsilateral side; Week*Group, $F_{5,63} = 3.03$, $p < 0.05$) where the control group performed with a significantly lower accuracy compared to all other groups (all, $p < 0.05$). However, over the following two blocks of post-surgery testing, all groups increased their response accuracy to ipsilateral stimuli to >80% and in the last block (LX-3) there was no difference in accuracy between all experimental groups (analysis restricted to ipsilateral side; Groups, $F_{5,63} = 2.18$, p = n.s.). Interestingly, albeit non-significant, animals of the moderate and 6-OHDA lesion groups performed with the highest response accuracy towards ipsilateral stimuli with 92% and 95% accuracy respectively. This could be most likely explained by the fact that these groups developed a bias towards this side of responding (discussed further below). At baseline, when analysing response accuracy towards stimuli presented on the side contralateral to the lesion, the GFP (93%) and 6-OHDA (94%) groups displayed a higher accuracy when compared to the other four experimental groups (>84%) (analysis restricted to the contralateral side; Group, $F_{5,63} = 5.57$, $p < 0.001$). In particular, the GFP group displayed a higher response accuracy than the control, noTG and h-aSYN mild group, whereas the 6-OHDA group performed with a higher response accuracy than the control, h-aSYN mild and h-aSYN moderate groups (all, $p < 0.05$). Again, both h-aSYN injected groups performed with an accuracy similar to the control and noTG groups (all, p = n.s.). After surgery, all injected groups performed with a lowered response accuracy towards contralateral stimuli (analysis restricted to the contralateral side; Week*Group, $F_{15,189} = 12.83$, $p < 0.001$). The control group performed with the highest accuracy during all three post-surgery blocks and at LX-3 achieved an accuracy similar to the baseline value (88%). The noTG group displayed a 22% reduction in response accuracy after the lesion which was significantly lower than the control group ($p < 0.001$) at LX-1 but recovered to pre-lesion performance (89%) and was not different from the control group (p = n.s.) at the last two blocks of assessment. The GFP injected group developed a deficit (67%) similar to the one observed in the noTG group at LX-1, which was also significantly lower than the control group ($p < 0.001$). Although the animals of the GFP group did improve (>81%), their response accuracy remained significantly lower than the one of the control groups at the last post-surgery timepoints (both, $p < 0.05$). This demonstrates the sensitivity of the operant assessment to detect small but significant differences which were not detected in all the other simple behavioural assessments reported above. Interestingly the accuracy of the three remaining groups did stay stable over the three post-surgery weeks of testing with the 6-OHDA lesion group being the most impaired. During all timepoints, animals of the 6-OHDA group performed with low accuracy towards contralateral stimuli (<7%) which was significantly different to all other groups at all time-points (all, $p < 0.001$). Animals of the h-aSYN moderate group were also severely impaired, albeit performed with a higher accuracy than the 6-OHDA lesioned animals, which was significantly lower than all three control and the h-aSYN mild group (all, $p < 0.001$). The h-aSYN mild group also displayed a stable accuracy deficit over the three post-surgery timepoints (<68%) which was significantly lower than all the three control groups at all timepoints assessed (all, $p < 0.001$). Furthermore, the contralateral response deficit correlated highly with the TH loss in the SN (Rho: −0.503, $p < 0.001$) which indicates a strong relationship between the two factors (Rea and Parker, 2014) (Fig. 4L).

In summary, animals that received h-aSYN or 6-OHDA injections developed a stable response bias towards ipsilateral stimuli which is reflected in the increased accuracy on the ipsilateral side and the decreased accuracy towards stimuli on the contralateral side. Furthermore, the operant task revealed similar stable deficits in the GFP injected animals. This is a powerful demonstration of the sensitivity of operant assessment where small deficits can be readily detected.

3.3.2.4. Reaction times. Reaction time was defined as the latency from presentation of the lateralised stimulus to the withdrawal of the nose from the central hole. All groups performed with fast reaction times during baseline acquisition (Fig. 4G-G_I). When animals had to react to stimuli presented to the ipsilateral side, there was no difference between the groups at any block of testing (analysis restricted to ipsilateral side; Week*Group, $F_{15,189} = 1.17$, p = n.s.). When the lateralised response was presented on the contralateral side, however, reaction times were significantly increased after the surgery for the 6-OHDA and h-aSYN moderate group (analysis restricted to contralateral side; Week*Group, $F_{15,189} = 3.51$, $p < 0.001$). Whereas animals of the control, noTG, GFP and h-aSYN mild group did react with a speed of 300 ms to contralateral stimuli (all, p = n.s.), animals of the 6-OHDA lesion group displayed increase reaction times of >600 ms for all three post-surgery timepoints, which was significantly different from the four above mentioned groups (all, $p < 0.01$). Animals of the moderate group displayed increased reaction times already at the first week of post-surgery assessment, however this increase only returned significant for the second (LX-2) and third block (LX-3) of post-surgery assessment (all, $p < 0.01$).

3.3.2.5. Movement times. Movement time was defined as the latency from withdrawal of the nose from the centre hole to the execution of the lateralised response (Fig. 4H-H_I). Before surgery, all animals performed the lateralised response rapidly (Group, $F_{5,63} = 0.95$, p = n.s.), and there was no difference between the side of response (Side, $F_{1,63} = 3.69$, p = n.s.). After vector delivery, there was a significant difference between groups in the latency to execute the lateralised response (Week*Side*Group, $F_{15,189} = 4.29$, $p < 0.001$). Although response latencies were increased in general after the surgery for some groups, this increase was more pronounced when responses had to be directed to the side contralateral to the lesion (Sides, $F_{1,63} = 10.60$, $p < 0.001$). Responses to

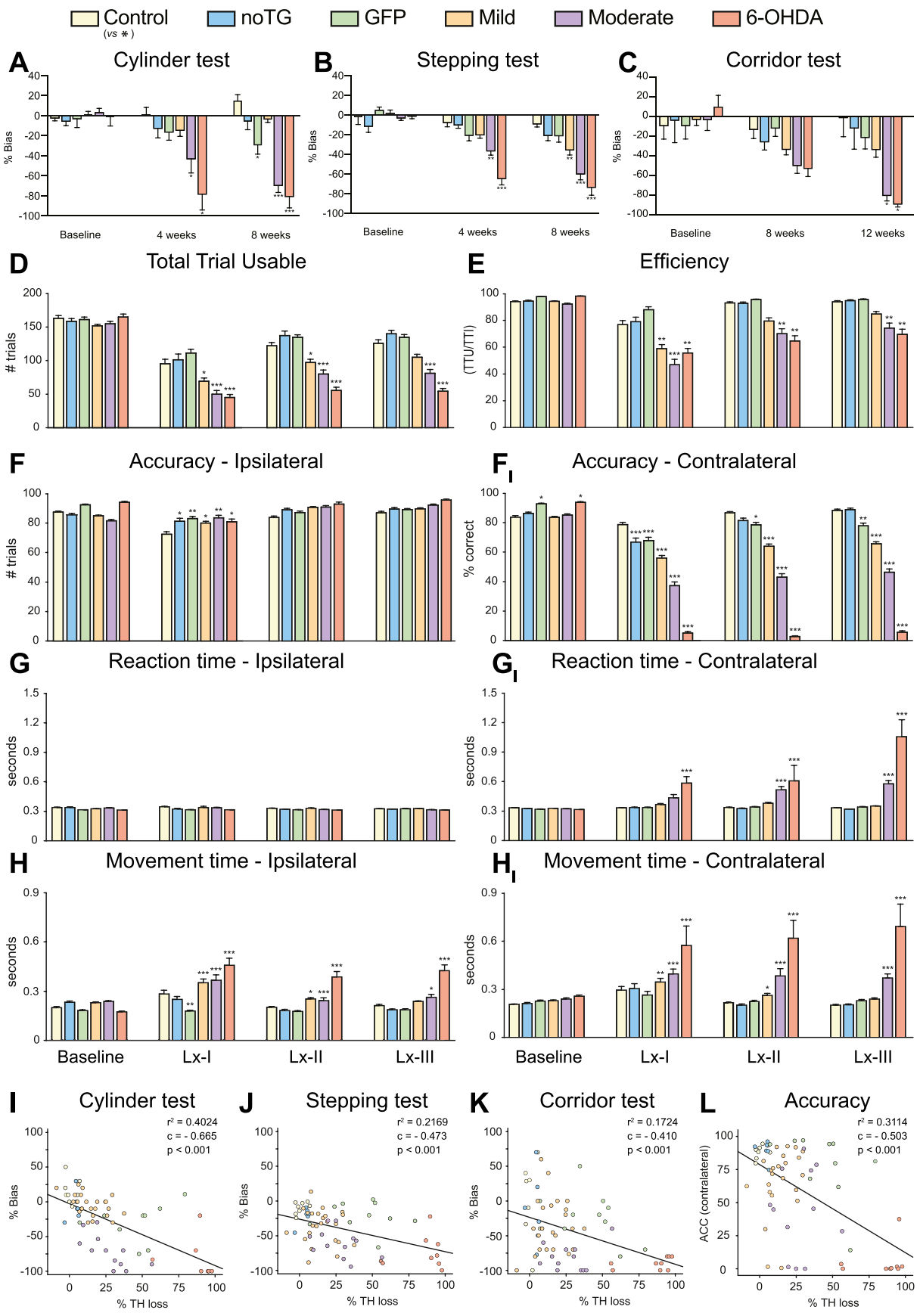

(caption on next page)

Fig. 4. Simple and complex behavioural assessment.
A-C: Cylinder (A) and stepping (B) tests were performed at baseline, 4- and 8- weeks post lesion for all the experimental groups. Corridor (C) test was performed at baseline, 8- and 12-weeks post lesion for all the experimental groups. **D:** Lateralised choice reaction time task total trial usable (TTU) for the baseline and for the 5-days blocks post-lesion (LX-1, LX-2, and LX-3. **E:** Lateralised choice reaction time task efficiency (EFF). **F-F_I:** Lateralised choice reaction time task accuracy (ACC) for ipsilateral (F) and contralateral (F_I) side. **G-G_I:** Lateralised choice reaction time task reaction time (RT) for stimuli presented at the ipsilateral (G) and contralateral (G_I) side. **H–H_I:** Lateralised choice reaction time task movement time (MT) for responses directed to the ipsilateral (H) and contralateral (H_I) side. The number of asterisks denotes significant differences at the <0.05, <0.01, and <0.001 levels of significance, respectively to the control group. All data are expressed as mean ± SEM. The full table of statistical cross comparison is provided in Supplementary Tables 2–12 for all behavioural tests. **I:** Scatterplot displaying the correlation between the loss of TH $^+$ cells as quantified by unbiased stereology and cylinder test contralateral bias. **J:** Scatterplot displaying the correlation between the loss of TH $^+$ cells quantified by unbiased stereology and bias on the stepping test. **K:** Scatterplot displaying the correlation between the loss of TH $^+$ cells as quantified by unbiased stereology and bias on the corridor test. **L:** Scatterplot displaying the correlation between the loss of TH^+ cells as quantified by unbiased stereology and contralateral accuracy. The number of asterisks denotes significant differences at the <0.05, <0.01, and <0.001 levels of significance, respectively. Differences from the respective groups are indicated by colour. All data are expressed as mean ± SEM.

the ipsilateral side were significantly prolonged (analysis restricted to ipsilateral side; Week*Group, $F_{15,189} = 1.86$, $p < 0.05$) for the h-aSYN mild and h-aSYN moderate groups, compared to the GFP group, at all post-surgery timepoints (all, $p < 0.05$). For the 6-OHDA lesion group, the execution of the lateralised response took twice as long as the three control groups at LX-1 (all, $p < 0.05$) and to all five groups at LX-2 and LX-3 (all, $p < 0.05$). When responses had to be executed on the contralateral side, response times were larger as well (analysis restricted to contralateral side; Week*Group, $F_{15,189} = 6.83$, $p < 0.001$). This increase was again most pronounced in the 6-OHDA lesion group which performed significantly slower compared to the three control groups at the first post-surgery timepoint (all, $p < 0.001$) and slower compared to all five groups at the second and third block of testing (all, $p < 0.001$). The h-aSYN mild group took longer to execute the lateralised response on the contralateral side compared to the three control groups at the first two post-surgery timepoints (both, $p < 0.05$), however at the final block of testing this group did not differ significantly anymore from the control, noTG and GFP groups. The h-aSYN moderate group did also display increased movement times for contralateral responses compared to the three control groups at all post-surgery timepoints (all, $p < 0.001$). Interestingly, during the second and third block of post-surgery testing the animals of the h-aSYN moderate group also performed significantly slower than animals of the h-aSYN mild group (both, $p < 0.05$).

3.4. Overexpression of h-aSYN leads to PD-like pathology in the striatum

In human PD, typical histopathological disease hallmarks include axonal neurodegeneration (Tagliaferro and Burke, 2016), followed by aSYN aggregations into Lewy neurites (LNs) and Lewy bodies (LBs) (Spillantini et al., 1998a, 1998b). Axonal degeneration occurs in the early phase of disease progression (Kordower et al., 2013; Hsiao et al., 2014; Kaasinen and Vahlberg, 2017). Using high magnification microscopy, we assessed histopathological markers of synucleinopathy in the TH^+ DA projections in the PFC and STR – two areas well known to receive the majority of midbrain DA projections from the Ventral Tegmental Area (VTA) and SN, respectively. In the PFC, very few detectable TH^+ swellings were visible for the control, noTG, GFP, or 6-OHDA (Fig. 5A–C, F). However, in both AAV-h-aSYN injected groups, we detected pathological axonal fibres (Fig. 5D and E). Quantifications in the PFC (Fig. 5Q) of these TH^+ swellings, revealed significant difference in the number of swellings between the groups (Fig. 5S; Group; $F_{5,56} = 2.42$ $p < 0.05$). Similarly, in the STR (Fig. 5G-L) we observed few TH^+ axonal swellings for the control, noTG, GFP and 6-OHDA group (Fig. 5G–I). In the STR of the h-aSYN mild and h-aSYN moderate groups we observed a strongly disrupted axonal network with abundant TH^+ swellings (Fig. 5J and K). The numbers of TH^+ axonal swellings analysed in three different areas of the STR (Fig. 5R) were different between the experimental groups (Group; $F_{5,60} = 7.25$, $p < 0.001$), with the most swellings observed in the moderate h-aSYN group (283 ± 43) and slightly fewer in the mild h-aSYN group (191 ± 37) (Fig. 5T). TH^+ swellings in both h-aSYN overexpressing groups were significantly higher than the control, noTG and 6-OHDA injected groups (both, $t > 3.178$, $p < 0.05$). Although there were some axonal swellings detected in the GFP injected group (Fig. 5I), these did not amount to statistically significant levels (Fig. 5T). The number of striatal TH^+ swellings per surviving nigral TH^+ DA neurons revealed that TH^+ swellings were twice as frequent in the AAV-h-aSYN moderate group (Fig. 5U), compared to the AAV-h-aSYN mild group; however no significant difference was observed between the two AAV-h-SYN groups, but only in relationship to the control group (Group; $F_{5,63} = 7.80$, $p < 0.001$).

Furthermore, abundant h-$aSYN^+$ swellings were detected in the PFC (Fig. 5M-N) and STR (Fig. 5O–P) of both AAV-h-aSYN groups. The number of h-aSYN swellings were significantly higher in the ipsilateral PFC and STR compared to the side contralateral to the injection for both, the mild and moderate groups (Fig. 5V–W; all $p < 0.05$). Interestingly, the number of swellings in the $aSYN^{211+}$ quantifications were twice as frequent as the comparative TH quantifications. This was the case in both the PFC and STR as well as for both AAV-h-aSYN injected groups, indicating that the majority of TH has been lost and corroborates the results obtained by the O.D. quantifications. Similarly to what observed using TH labelling, h-aSYN + swellings per surviving nigral TH $^+$ DA neurons (Fig. 5X) did not reveal any differences among the mild and moderate AAV-h-aSYN group ($t_{24} = 0.79$, p = n.s.).

To characterise the composition of these axonal swellings we used high magnification confocal imaging. The majority of striatal DA fibres displayed a beaded dystrophic and swollen morphology (Fig. 6A-B_{III}). This is a stage in the degenerative progress before segmentation and fragmentation into spheroids (Zhou et al., 1998). We also found that most of the TH^+ (Fig. 6A and B) and $VMAT2^+$ (Fig. 6A_I) dystrophic structures contained h-aSYN (Fig. 6B_I) which was also phosphorylated (Fig. 6A_{II}-B_{II}), similarly to what is seen in the midbrain cell bodies reported previously (Fig. 2P-P_{III}). Furthermore, the axonal h-aSYN swellings were resistant to proteinase K digestion (Supplementary Figs. 3A–B).

The cell bodies of remaining midbrain DA cells in the ipsilateral SN also presented with insoluble h-aSYN and displayed a pathological morphology with punctate granular deposits and cytoplasmic inclusions (Fig. 6C–F). The majority of remaining midbrain DA neurons also displayed a clear colocalization of nuclear DAPI with ThioflavinS and pSer129 (Fig. 6G-G_{III}). The presence of phosphorylated aSYN with an amyloid conformation suggests the presence of LBs-like structures that are very similar to the LBs seen and analysed in human PD patients (Hayashida et al., 1993; Arima et al., 1998; Duda et al., 2000; Giasson et al., 2000; Huang and Halliday, 2013; Irwin et al., 2013; Fares et al., 2021). In summary, our data suggests a pathological effect of h-aSYN overexpression on striatal DA axonal projections. Interestingly, such axonal pathology seen in our preclinical model of h-aSYN-based AAV overexpression, closely resembles pathological features that are observed in humans PD patients (Hayashida et al., 1993; Giasson et al., 2000).

It is widely accepted that in PD brains there is an interaction between neurodegeneration and inflammation, and that neurodegeneration might be the result of abundant pathological aSYN (Beraud et al., 2013; Codolo et al., 2013) coinciding with markers of neuroinflammation.

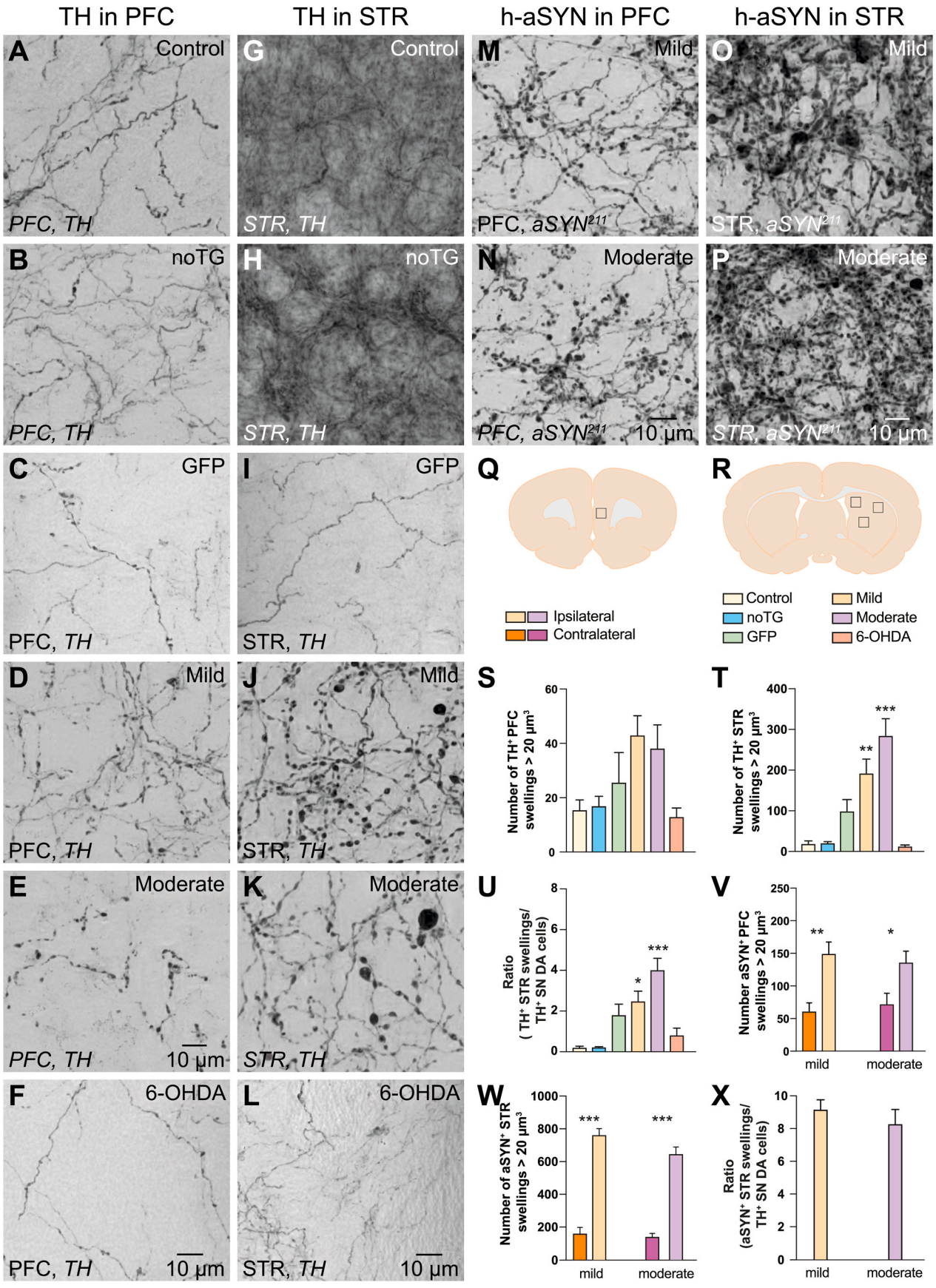

(caption on next page)

Fig. 5. Striatal axonal pathology following AAV delivery at 16 weeks post injection.
A-F: Representative brightfield photomicrographs of PFC axonal swellings in the ipsilateral PFC labelled for TH for the control (A), noTG (B), GFP (C) h-aSYN mild (D), h-aSYN moderate (E) and 6-OHDA (F) groups. **G-L:** Representative brightfield photomicrographs of striatal axonal swellings in the ipsilateral STR labelled for TH for the control (G), noTG (H), GFP (I) h-aSYN mild (J), h-aSYN moderate (K) and 6-OHDA (L) groups. **M-N:** Representative brightfield photomicrographs of PFC axonal swellings in the ipsilateral PFC labelled for $aSYN^{211}$ for the h-aSYN mild (M) and h-aSYN moderate (N) groups. **O–P:** Representative brightfield photomicrographs of STR axonal swellings in the ipsilateral STR labelled for $aSYN^{211}$ for the h-aSYN mild (o) and h-aSYN moderate (p) groups. **O–P:** Schematic representation of the analysed area for the PFC (Q) and STR (R). Black squares indicate the areas where image acquisition was performed. **S:** Quantification of TH^+ swellings in the ipsilateral PFC for all the experimental groups. Data are presented as mean ± SEM. **T:** Quantification of TH^+ swellings in the ipsilateral STR for all the experimental groups. Data are presented as mean ± SEM; ** = $p < 0.01$; *** = $p < 0.001$. Significance is expressed in relation to the control group. **U:** Ratio between number of TH^+ STR swellings and remaining TH^+ DA nigral neurons. Data are presented as mean ± SEM; * = $p < 0.05$; *** = $p < 0.001$. Significance is expressed in relation to the control group. **V:** Quantification of $aSYN^{211+}$ swellings in the ipsilateral and contralateral PFC for the h-aSYN mild and h-aSYN moderate groups. Data are presented as mean ± SEM; * = $p < 0.05$; ** = $p < 0.01$. **W:** Quantification of $aSYN^{211+}$ swellings in the ipsilateral and contralateral STR for the h-aSYN mild and h-aSYN moderate groups. Data are presented as mean ± SEM; *** = $p < 0.001$. **X:** Ratio between number of $aSYN^{211+}$ STR swellings and remaining TH^+ DA nigral neurons. Data are presented as mean ± SEM.

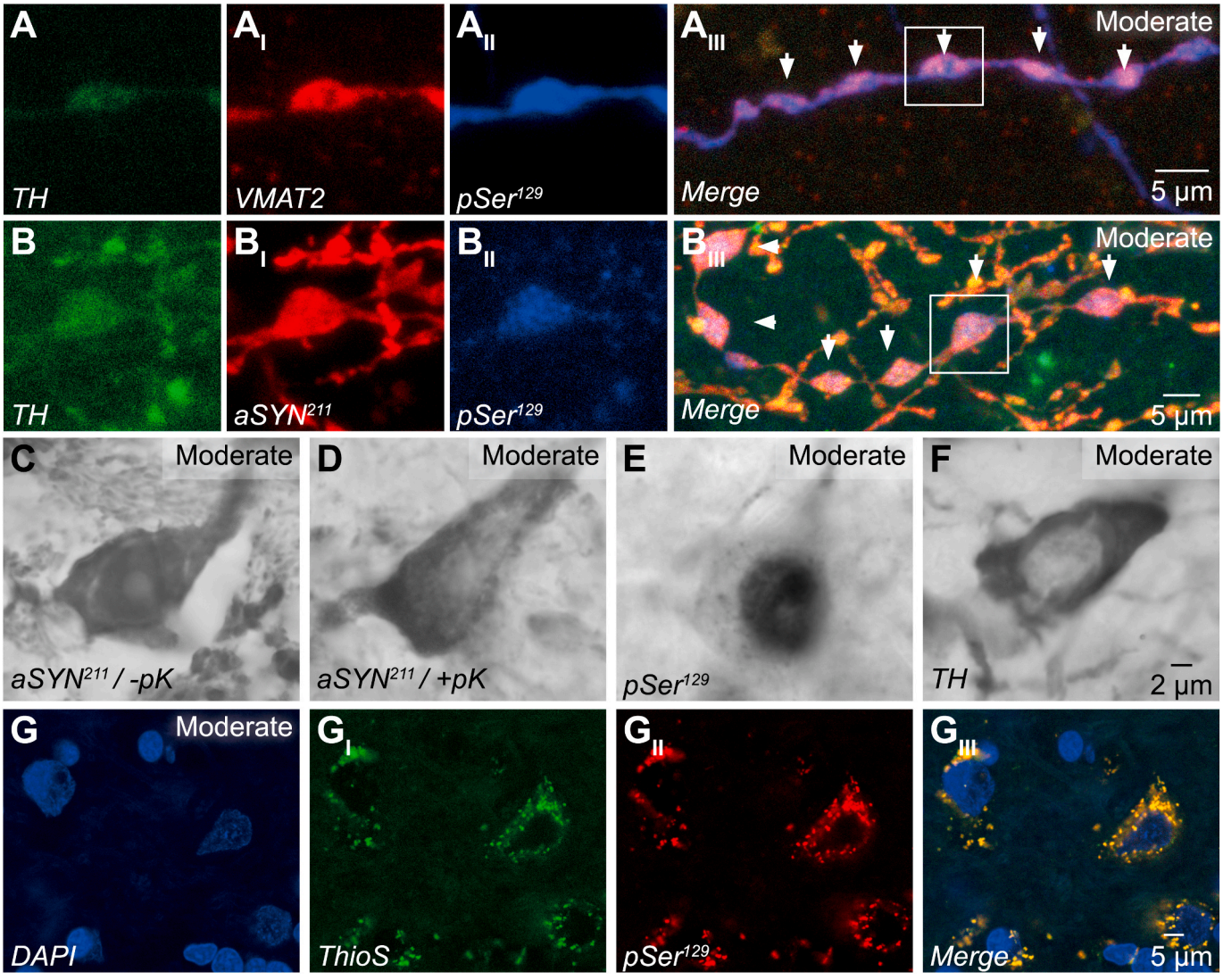

Fig. 6. Axonal and nigral pathology following AAV delivery at 16 weeks post injection.
A-B_{III}: Representative high magnification confocal images of the h-aSYN moderate ipsilateral striatal swellings presenting with beaded morphology labelled for TH (A, B) VMAT2 (A_I) or $aSYN^{211}$ (B_I) and $pSer^{129}$ (A_{II}, B_{II}). **C-D:** High magnification images of midbrain cellular pathology and protein accumulation revealed by $aSYN^{211}$ immunoreactivity without (C) or with pK treatment (D). **E-F:** High magnification images of midbrain cellular pathology and protein accumulation revealed by $pSer^{129}$ (E) and TH (F) immunoreactivity. **G-G_{III}:** Representative triple fluorescent labelling of DAPI (G), ThioS (G_I) and $pSer^{129}$ (G_{II}) displaying co-localization of phosphorylated aSYN with protein aggregates known to be present in human LBs.

However, it is not clear if inflammation is the cause or consequence (or both) of neuronal toxicity (McGeer and McGeer, 2004; Phani et al., 2012; Caggiu et al., 2019; Marogianni et al., 2020). To better frame the pathology undergoing in our developed model, we investigated whether high levels of h-aSYN overexpression in the midbrain would coincide with a neuroinflammatory response and consequent microglial activation. DAB-IHC in the midbrain for the ionized calcium-binding adaptor molecule 1 (IBA1) revealed a localized increase of $IBA1^+$ cells in the

ipsilateral hemisphere of the animals receiving intranigral delivery of either AAV or neurotoxin; this was not evident for the uninjected control group (Supplementary Figs. 4A–F). High magnification images of IBA1$^+$ cell morphology did not reveal any apparent changes in the cells' soma or processes indicative of an activated state of inflammation between the ipsilateral and contralateral hemisphere, as well as between different groups (Supplementary Fig. 4A$_I$-F$_{II}$, G). Quantification of midbrain IBA1$^+$ microglial cells number (Supplementary Fig. 4H) revealed that the average number of cells in both ipsilateral and contralateral hemisphere did not differ statistically for animals of the control group ($t_7 = 0.95$, p = n.s.). Interestingly, all the groups who received surgery, irrespective of substance injected, displayed a similar increase in the number of IBA1$^+$ cells (all, $t > 3.15$, $p < 0.05$), which can most likely be ascribed to the surgical procedure, rather than an ongoing inflammatory response. As only a single time-point was analysed, we cannot exclude the possibility of an earlier inflammatory response which declined over time. Previously, such an early activation has been reported in response to aSYN overexpression (4 weeks post-surgery) (Theodore et al., 2008; Sanchez-Guajardo et al., 2010). High magnification confocal microscopy for IBA1 confirmed that the microglial cells are not in a hyperactivated morphological conformation, but rather in a semi-ramified state, with a relatively small soma and branches extended in the surrounding area (Supplementary Fig. 4G). Triple FL-IHC for TH, IBA1 and h-aSYN (Supplementary Fig. 4I-I$_{III}$) displays a microglial cell in close apposition to the cell body of a TH$^+$ DA neuron that also contains h-aSYN. This suggests that even if microglial cells do not undergo specific morphological changes, they might recognize h-aSYN as a potential disruptor of physiological conditions and localizes in close proximity of h-aSYN expressing cells.

4. Discussion

In the present work we utilized a viral vector approach to overexpress h-aSYN in the midbrain of rats to model both motor and non-motor deficits in a preclinical rodent model of PD. AAV-h-aSYN overexpression models result in more variability in the success-rate of producing animals with stable behavioural deficits (Yamada et al., 2004; Chung et al., 2009; Decressac et al., 2012a, 2012b; Gubinelli et al., 2022; Negrini et al., 2022); this is an important limitation in preclinical studies that depend on stable behavioural deficits that are not prone to spontaneous recovery. In the present study, it was possible to identify animals with a moderate cellular loss in the midbrain DA system based on combined deficits of the cylinder, stepping and corridor test (all >20% bias (Grealish et al., 2010)) as well as the choice reaction time task, with the latter two being the most discriminative. This is the first report on a complex motor control task in the AAV-h-aSYN overexpression model and provides for a fuller characterisation of the behavioural deficits thereof. Although the simple tests of motor function are commonly used (Deumens et al., 2002), the pattern of movement deficits in humans is considerably more complex than what is measured on these tests of spontaneous motor function. Two of the cardinal symptoms of parkinsonism is bradykinesia (Jankovic, 2008; Obeso et al., 2017) (decreased movement velocity) and akinesia (difficulty in movement initiation). In the current study we employed a choice reaction time task that enables us to dissociate the time to initiate movement (reaction time) from the time taken to execute the lateralised response (movement time), hence two parameters analogous to akinesia and bradykinesia of the human condition, respectively. Deficits in simple and choice reaction times have repeatedly been reported in human PD patients (Evarts et al., 1981; Jahanshahi et al., 1992; Gauntlett-Gilbert and Brown, 1998). Moreover, rodents with unilateral 6-OHDA lesions display deficits in simple and choice reaction time tasks (Brown & Robbins, 1989a, 1991; Carli et al., 1989; Baunez and Robbins, 1999; Phillips and Brown, 1999; Heuer and Dunnett, 2012, 2013; Heuer et al., 2013a, 2013b, 2013c). In the current study, rats of the h-aSYN moderate and the 6-OHDA lesion group displayed increased reaction times when the lateralised stimulus was presented contralateral to the animal's head, hence providing for the first time in a synucleinopathy model an account of a deficit in movement initiation. Movement times were increased in both AAV-h-aSYN groups as well as the 6-OHDA group bilaterally, although more pronounced for responses directed into contralateral space. Similar to the 6-OHDA lesion model, AAV-h-aSYN overexpression led to motivational deficits as indicated by the number of initiated trials (TTU). As described previously, the initial response to the centre hole remains goal directed even after extensive periods of training and is affected by outcome devaluation or reward omission. In contrast, the lateralised response becomes habitual and governed by stimulus-response associations (Wise, 2004; Lelos et al., 2012). Furthermore, rats of the AAV-GFP, AAV-h-aSYN mild, and AAV-h-aSYN moderate group as well as the 6-OHDA lesion group displayed a deficit in contralateral accuracy. This lateralised attentional neglect has previously been reported only in 6-OHDA lesions (Dowd and Dunnett, 2004, 2005b; a, 2007; Lelos et al., 2012; Heuer et al., 2013a). The accuracy deficit towards contralateral response locations is interpreted as an attentional deficit in contralateral space, and when responses were restricted only towards the contralateral side, but providing a near and a far contralateral response location, rats were perfectly capable of responding to the previously neglected response hole and neglecting the contralateral far location (Brown and Robbins, 1989b; a, 1991; Heuer and Dunnett, 2013; Heuer et al., 2013a). Our observed deficit was shown to be stable for 50 days post-lesion and concurrent probe trials which varied the distance and location of the near and far hole did not change the response pattern, i.e., the bias towards the most proximal location (Heuer and Dunnett, 2013; Heuer et al., 2013a). These data exclude a deficit which is due to a primary deficit in sensory perception nor execution of a motoric response *per se*, but rather a deficit in relative egocentric space. Cognitive deficits have only been modelled in AAV-h-aSYN or pre-formed fibrils (PFFs) injection models with limited success, e.g., spatial working and reference memory on the Morris water maze test when aSYN was overexpressed in the VTA and septum (Hall et al., 2013) or following injection of PFFs into the hippocampus (Kasongo et al., 2020). AAV-h-aSYN overexpression in both neonate mice and rats has generally led to the development of pathology, but not to robust deficits in non-motor domains (Aldrin-Kirk et al., 2014; Delenclos et al., 2017). We have previously shown minor deficits on working memory on a delayed matching to position task after combined aSYN and PFFs injection into the PFC (Espa et al., 2019). The operant task utilized in the present work is sensitive enough to detect small behavioural differences in the control groups (AAV-noTG and AAV-GFP) (Carli et al., 1989; Brown and Robbins, 1991; Dowd and Dunnett, 2005a; Heuer and Dunnett, 2012, 2013).

In the current study, the TH loss obtained by AAV-h-aSYN overexpression was similar to that observed by previous reports from our and other groups (Chung et al., 2009; Koprich et al., 2010; Decressac et al., 2011, 2012a, 2012b; Lundblad et al., 2012; Gombash et al., 2013; Oliveras-Salva et al., 2013; Van der Perren et al., 2015; Gubinelli et al., 2022; Negrini et al., 2022).

Interestingly, even though AAV-GFP injected animals displayed a larger nigral cell loss compared to the AAV-h-aSYN injected groups, the behavioural deficits were smaller. This is indicative that cellular loss is not the only factor responsible for the behavioural deficit. In the classical neurotoxicant 6-OHDA model animals with <60% TH$^+$ cell loss in the SN usually do not present with stable behavioural deficits (Kirik et al., 1998; Truong et al., 2006). These animals might display a minor deficit which recovers after repeated testing to pre-lesion performance and the deficit can be re-instated by injection of the tyrosine-hydroxylase inhibitor alpha-*methyl*-para-tyrosine (Dowd and Dunnett, 2005a). The biological mechanisms for the recovery are thought to be sprouting of remaining host fibres, an upregulation of DA release, and an upregulation of post-synaptic DA receptors (Acheson and Zigmond, 1981; Robinson and Whishaw, 1988). In the AAV-GFP group we do not detect the levels of axonal pathology in form of swellings and inclusion formation that is present in animals where h-aSYN was

overexpressed. Indeed, impairments in DA release and reuptake kinetics has been repeatedly demonstrated repeatedly after h-aSYN overexpression (Lundblad et al., 2012; Hansen et al., 2013; Thakur et al., 2017; Gubinelli et al., 2022). Although GFP is the most used control protein, there are several concerns regarding its use. GFP is derived from a non-mammalian species (Aequorea Victoria jellyfish) (Ormo et al., 1996) and the immune-response towards non-self-proteins has to be taken into account (for an excellent review on the choice of an appropriate control vector we refer to (Albert et al., 2017)). GFP toxicity has been reported by several authors (Klein et al., 2006; Koprich et al., 2011; Landeck et al., 2017; Albert et al., 2019; Negrini et al., 2022). An additional reason for the variation in GFP toxicity seen in the literature could be explained by the method used for virus titration; in a previous study we have discussed variation in production methodologies and QC as a potential source of variability in GFP toxicity (Gubinelli et al., 2022). We believe that the lack of a behavioural deficit in the AAV-GFP group is due to two main reasons: first, the level of degeneration was not sufficient to induce behavioural deficits on its own and second, the integrity of the remaining host-fibres could provide some compensatory mechanisms such as upregulation of DA production, sprouting of remaining TH fibres or changes in post-synaptic sensitivity (Acheson and Zigmond, 1981; Robinson and Whishaw, 1988). The AAV-h-aSYN moderate group displayed a similar loss of nigral TH^+ DA neurons, but a stable and significant deficit on all behavioural tasks. The morphological analysis of striatal fibres revealed the presence of dystrophic axons with clear signs of synucleinopathy (presence of soluble and insoluble phosphorylated forms of aSYN), as well as the presence of nigral DA-$aSYN^+$ aggregates. The axonal pathology detected, together with demonstrations of impaired DA release and reuptake kinetics from our previous work (Lundblad et al., 2012; Gubinelli et al., 2022; Negrini et al., 2022) suggest that in these protein-overexpression models the axonal pathology of remaining host fibres is an important contributor to the development of behavioural impairments. Indeed, it has been suggested that DA neurodegeneration starts in the DA terminals and not in the midbrain DA cells and AAV-h-aSYN overexpression can induce significant striatal terminal loss without nigral neuronal depletion (Sanchez-Guajardo et al., 2010). Disrupted neuronal transmission and degeneration of terminals after AAV-h-aSYN overexpression has also been shown to induce motor impairments in rats (Phan et al., 2017) and primates (Eslamboli et al., 2007) even without significant neuronal loss. This is also in accordance with PD human data, where depletion of TH^+ fibres in the putamen precedes the degeneration of nigral cell bodies (Kordower et al., 2013; Kurowska et al., 2016).

One major issue with the use of AAV vector models is the variability within experimental groups even when excluding between group differences such as AAV serotype, purification method, promotor, transgene, stabilizing sequences, gc-titer and titration method, volume injected, site of injection, promotor, protein-stabilizing sequences, etc.

AAV vector models have been reported to produce much greater variation (Kirik et al., 2002; Yamada et al., 2004; Maingay et al., 2006; Gorbatyuk et al., 2008; Chung et al., 2009; Decressac et al., 2012a, 2012b), especially when compared to neurotoxicant injections models (e.g. 6-OHDA into the MFB), where the lesion success rate is usually >90% (Torres et al., 2011). Although the SN is a small nucleus deep in the brain, from the vector expression data we can assume that most of the animals were targeted correctly. As the striatum is a heterogeneous structure (Collins and Saunders, 2020) differences in degeneration of innervating striatal fibres will affect behaviours differently between rats within the same experimental group. This is the analogue of the classical 6-OHDA intrastriatal injections where although the terminal fibre field is depleted, there is greater variability in surviving midbrain cell bodies.

Despite the neurotoxicity of the GFP control group in the present study, the development of key histopathological hallmarks of human PD histopathology was only limited to the h-aSYN overexpression groups. The Lewy-body-like structures displayed proteinase K-resistant cytoplasmic inclusions, as well as the formation of $pSer^{129}$-labelled cell bodies in the midbrain and neurites in the striatum and PFC. We observed axonal pathology consisting of beaded and fragmented axons that were positively labelled for TH, VMAT2, human aSYN and $pSer^{129}$. Overall, the histopathological assessment, including $pSer^{129}$ and Thioflavin S as well as proteinase K-resistant aggregates confirms the formation of Lewy-like pathology in our model (Fujiwara et al., 2002; Anderson et al., 2006; Wakabayashi et al., 2007, 2013; Dickson, 2018).

In this work we used an empty vector as an additional control, demonstrating that such vector does not lead to detectable TH cell loss via unbiased stereology; however, this does not facilitate the evaluation of the general effects of protein overexpression. Alternative approaches such as overexpression of vectors carrying an inducible transgene cassette or scrambled h-aSYN genome might be used (Koprich et al., 2016; Musacchio et al., 2017; Albert et al., 2019; Alarcon-Aris et al., 2020).

In the present study we could not link the neurodegeneration or development of pathology to an inflammatory response in the brain, despite the increase in the number of microglial cells at the site of injection in all groups receiving surgery. Morphologically the microglial cells remained in a ramified or rod-like state and did not display overt signs of activated or amoeboid morphology. Whether such an inflammatory response had taken place at an earlier timepoint was not assessed. Previous studies of shorter assessment periods have reported such a relation (Su et al., 2008, 2009; Chung et al., 2009; Kim et al., 2009; Sanchez-Guajardo et al., 2010).

In the 6-OHDA lesion model much higher levels of nigral DA neuron loss are necessary to induce stable behavioural deficits (>50–60% TH loss (Kirik et al., 1998)), as partially lesioned 6-OHDA animals are prone to compensatory sprouting and spontaneous recovery (Dravid et al., 1984; Onn et al., 1986; Liberatore et al., 1999; Finkelstein et al., 2000). In the h-aSYN overexpression model we were able to select animals, based on a behavioural deficit of >20% on a combination of cylinder, stepping and corridor test, that presented TH cell loss and stable behavioural deficits. These animals are suitable for assessment of therapeutic approaches such as cell replacement therapy or gene therapy.

CRediT authorship contribution statement

F. Gubinelli: Data curation, Formal analysis, Writing – original draft, revisions. **L. Sarauskyte:** Data curation, Formal analysis. **C. Venuti:** Data curation, Formal analysis. **I. Kulacz:** Data curation, Formal analysis. **G. Cazzolla:** Data curation, Formal analysis. **M. Negrini:** Data curation, Formal analysis. **D. Anwer:** Data curation, Formal analysis. **I. Vecchio:** Data curation, Formal analysis. **F. Jakobs:** Data curation, Formal analysis. **F.P. Manfredsson:** experimental design, Writing – original draft, revisions. **M. Davidsson:** Data curation, Formal analysis, Writing – original draft, revisions, experimental design. **A. Heuer:** Data curation, Formal analysis, Writing – original draft, revisions, experimental design, Funding acquisition. All authors approve the final version of the manuscript.

Declaration of competing interest

The authors declare that they have no known competing financial interests or personal relationships that could have appeared to influence the work reported in this paper.

Data availability

Data will be made available on request.

Acknowledgement

We would like to thank Elena Espa assistance with the proteinase K treatment. MD was supported by a post-doctoral fellowship from Birgit and Hellmuth Hertz Foundation. FPM would like to acknowledge

funding support from NIH/NIDDK R01DK108798 as well as funding from DOD, the NIH/NINDS, the Michael J Fox Foundation and the Parson's Foundation. AH would like to acknowledge generous funding by the Swedish Research Council (VR2016-01789), Demensförbundet, the Crafoord foundation, the Gyllenstiernska Krapperupsstiftelsen, the Thorsten and Elsa Segerfalks Stiftelsen, the Royal Physiographic Society in Lund, the Swedish Parkinson Foundation (Parkinsonsfonden), the Fredrik och Ingrid Thurings Stiftelsen, the Swedish Society of Medicine (SSMF), the Åhlensstiftelsen, the Hedlundsstiftelsen, the Svenska Läkaresällskapet and the Jeansonsstiftelsen.

Appendix A. Supplementary data

Supplementary data to this article can be found online at https://doi.org/10.1016/j.crneur.2022.100065.

References

Acheson, A.L., Zigmond, M.J., 1981. Short and long term changes in tyrosine hydroxylase activity in rat brain after subtotal destruction of central noradrenergic neurons. J. Neurosci. 1, 493–504.

Alarcon-Aris, D., Pavia-Collado, R., Miquel-Rio, L., Coppola-Segovia, V., Ferres-Coy, A., Ruiz-Bronchal, E., Galofre, M., Paz, V., Campa, L., Revilla, R., Montefeltro, A., Kordower, J.H., Vila, M., Artigas, F., Bortolozzi, A., 2020. Anti-alpha-synuclein ASO delivered to monoamine neurons prevents alpha-synuclein accumulation in a Parkinson's disease-like mouse model and in monkeys. EBioMedicine 59, 102944.

Albert, K., Voutilainen, M.H., Domanskyi, A., Airavaara, M., 2017. AAV vector-mediated gene delivery to substantia nigra dopamine neurons: implications for gene therapy and disease models. Genes (Basel) 8.

Albert, K., Voutilainen, M.H., Domanskyi, A., Piepponen, T.P., Ahola, S., Tuominen, R.K., Richie, C., Harvey, B.K., Airavaara, M., 2019. Downregulation of tyrosine hydroxylase phenotype after AAV injection above substantia nigra: caution in experimental models of Parkinson's disease. J. Neurosci. Res. 97, 346–361.

Aldrin-Kirk, P., Davidsson, M., Holmqvist, S., Li, J.Y., Bjorklund, T., 2014. Novel AAV-based rat model of forebrain synucleinopathy shows extensive pathologies and progressive loss of cholinergic interneurons. PLoS One 9, e100869.

Anderson, J.P., Walker, D.E., Goldstein, J.M., de Laat, R., Banducci, K., Caccavello, R.J., Barbour, R., Huang, J., Kling, K., Lee, M., Diep, L., Keim, P.S., Shen, X., Chataway, T., Schlossmacher, M.G., Seubert, P., Schenk, D., Sinha, S., Gai, W.P., Chilcote, T.J., 2006. Phosphorylation of Ser-129 is the dominant pathological modification of alpha-synuclein in familial and sporadic Lewy body disease. J. Biol. Chem. 281, 29739–29752.

Arima, K., Ueda, K., Sunohara, N., Hirai, S., Izumiyama, Y., Tonozuka-Uehara, H., Kawai, M., 1998. Immunoelectron-microscopic demonstration of NACP/alpha-synuclein-epitopes on the filamentous component of Lewy bodies in Parkinson's disease and in dementia with Lewy bodies. Brain Res. 808, 93–100.

Baunez, C., Robbins, T.W., 1999. Effects of dopamine depletion of the dorsal striatum and further interaction with subthalamic nucleus lesions in an attentional task in the rat. Neuroscience 92, 1343–1356.

Beraud, D., Hathaway, H.A., Trecki, J., Chasovskikh, S., Johnson, D.A., Johnson, J.A., Federoff, H.J., Shimoji, M., Mhyre, T.R., Maguire-Zeiss, K.A., 2013. Microglial activation and antioxidant responses induced by the Parkinson's disease protein alpha-synuclein. J. Neuroimmune Pharmacol. 8, 94–117.

Boller, F., Passafiume, D., Keefe, N.C., Rogers, K., Morrow, L., Kim, Y., 1984. Visuospatial impairment in Parkinson's disease. Role of perceptual and motor factors. Arch. Neurol. 41, 485–490.

Brasted, P.J., Dobrossy, M.D., Robbins, T.W., Dunnett, S.B., 1998. Striatal lesions produce distinctive impairments in reaction time performance in two different operant chambers. Brain Res. Bull. 46, 487–493.

Brasted, P.J., Humby, T., Dunnett, S.B., Robbins, T.W., 1997. Unilateral lesions of the dorsal striatum in rats disrupt responding in egocentric space. J. Neurosci. 17, 8919–8926.

Brown, V.J., Robbins, T.W., 1989a. Deficits in response space following unilateral striatal dopamine depletion in the rat. J. Neurosci. 9, 983–989.

Brown, V.J., Robbins, T.W., 1989b. Elementary processes of response selection mediated by distinct regions of the striatum. J. Neurosci. 9, 3760–3765.

Brown, V.J., Robbins, T.W., 1991. Simple and choice reaction time performance following unilateral striatal dopamine depletion in the rat. Impaired motor readiness but preserved response preparation. Brain 114 (Pt 1B), 513–525.

Caggiu, E., Arru, G., Hosseini, S., Niegowska, M., Sechi, G., Zarbo, I.R., Sechi, L.A., 2019. Inflammation, infectious triggers, and Parkinson's disease. Front. Neurol. 10, 122.

Carli, M., Evenden, J.L., Robbins, T.W., 1985. Depletion of unilateral striatal dopamine impairs initiation of contralateral actions and not sensory attention. Nature 313, 679–682.

Carli, M., Jones, G.H., Robbins, T.W., 1989. Effects of unilateral dorsal and ventral striatal dopamine depletion on visual neglect in the rat: a neural and behavioural analysis. Neuroscience 29, 309–327.

Carli, M., Robbins, T.W., Evenden, J.L., Everitt, B.J., 1983. Effects of lesions to ascending noradrenergic neurones on performance of a 5-choice serial reaction task in rats; implications for theories of dorsal noradrenergic bundle function based on selective attention and arousal. Behav. Brain Res. 9, 361–380.

Chung, C.Y., Koprich, J.B., Siddiqi, H., Isacson, O., 2009. Dynamic changes in presynaptic and axonal transport proteins combined with striatal neuroinflammation precede dopaminergic neuronal loss in a rat model of AAV alpha-synucleinopathy. J. Neurosci. 29, 3365–3373.

Codolo, G., Plotegher, N., Pozzobon, T., Brucale, M., Tessari, I., Bubacco, L., de Bernard, M., 2013. Triggering of inflammasome by aggregated alpha-synuclein, an inflammatory response in synucleinopathies. PLoS One 8, e55375.

Collins, A.L., Saunders, B.T., 2020. Heterogeneity in striatal dopamine circuits: form and function in dynamic reward seeking. J. Neurosci. Res. 98, 1046–1069.

Cresto, N., Gardier, C., Gaillard, M.C., Gubinelli, F., Roost, P., Molina, D., Josephine, C., Dufour, N., Auregan, G., Guillermier, M., Bernier, S., Jan, C., Gipchtein, P., Hantraye, P., Chartier-Harlin, M.C., Bonvento, G., Van Camp, N., Taymans, J.M., Cambon, K., Liot, G., Bemelmans, A.P., Brouillet, E., 2021. The C-terminal domain of LRRK2 with the G2019S substitution increases mutant A53T α-synuclein toxicity in dopaminergic neurons in vivo. Int. J. Mol. Sci. 22.

Davidsdottir, S., Cronin-Golomb, A., Lee, A., 2005. Visual and spatial symptoms in Parkinson's disease. Vis. Res. 45, 1285–1296.

Davidsson, M., Negrini, M., Hauser, S., Svanbergsson, A., Lockowandt, M., Tomasello, G., Manfredsson, F.P., Heuer, A., 2020. A comparison of AAV-vector production methods for gene therapy and preclinical assessment. Sci. Rep. 10, 21532.

Decressac, M., Mattsson, B., Bjorklund, A., 2012a. Comparison of the behavioural and histological characteristics of the 6-OHDA and alpha-synuclein rat models of Parkinson's disease. Exp. Neurol. 235, 306–315.

Decressac, M., Mattsson, B., Lundblad, M., Weikop, P., Bjorklund, A., 2012b. Progressive neurodegenerative and behavioural changes induced by AAV-mediated overexpression of alpha-synuclein in midbrain dopamine neurons. Neurobiol. Dis. 45, 939–953.

Decressac, M., Ulusoy, A., Mattsson, B., Georgievska, B., Romero-Ramos, M., Kirik, D., Bjorklund, A., 2011. GDNF fails to exert neuroprotection in a rat alpha-synuclein model of Parkinson's disease. Brain 134, 2302–2311.

Delenclos, M., Faroqi, A.H., Yue, M., Kurti, A., Castanedes-Casey, M., Rousseau, L., Phillips, V., Dickson, D.W., Fryer, J.D., McLean, P.J., 2017. Neonatal AAV delivery of alpha-synuclein induces pathology in the adult mouse brain. Acta Neuropathol Commun 5, 51.

Deumens, R., Blokland, A., Prickaerts, J., 2002. Modeling Parkinson's disease in rats: an evaluation of 6-OHDA lesions of the nigrostriatal pathway. Exp. Neurol. 175, 303–317.

Dickson, D.W., 2018. Neuropathology of Parkinson disease. Park. Relat. Disord. 46 (Suppl. 1), S30–S33.

Dowd, E., Dunnett, S.B., 2004. Deficits in a lateralized associative learning task in dopamine-depleted rats with functional recovery by dopamine-rich transplants. Eur. J. Neurosci. 20, 1953–1959.

Dowd, E., Dunnett, S.B., 2005a. Comparison of 6-hydroxydopamine-induced medial forebrain bundle and nigrostriatal terminal lesions in a lateralised nose-poking task in rats. Behav. Brain Res. 159, 153–161.

Dowd, E., Dunnett, S.B., 2005b. Comparison of 6-hydroxydopamine-induced medial forebrain bundle and nigrostriatal terminal lesions in rats using a lateralised nose-poking task with low stimulus-response compatibility. Behav. Brain Res. 165, 181–186.

Dowd, E., Dunnett, S.B., 2007. Movement without dopamine: striatal dopamine is required to maintain but not to perform learned actions. Biochem. Soc. Trans. 35, 428–432.

Dowd, E., Monville, C., Torres, E.M., Dunnett, S.B., 2005a. The Corridor Task: a simple test of lateralised response selection sensitive to unilateral dopamine deafferentation and graft-derived dopamine replacement in the striatum. Brain Res. Bull. 68, 24–30.

Dowd, E., Monville, C., Torres, E.M., Wong, L.F., Azzouz, M., Mazarakis, N.D., Dunnett, S.B., 2005b. Lentivector-mediated delivery of GDNF protects complex motor functions relevant to human Parkinsonism in a rat lesion model. Eur. J. Neurosci. 22, 2587–2595.

Dravid, A., Jaton, A.L., Enz, A., Frei, P., 1984. Spontaneous recovery from motor asymmetry in adult rats with 6-hydroxydopamine-induced partial lesions of the substantia nigra. Brain Res. 311, 361–365.

Duda, J.E., Lee, V.M., Trojanowski, J.Q., 2000. Neuropathology of synuclein aggregates. J. Neurosci. Res. 61, 121–127.

Dunnett, S.B., 1985. Comparative effects of cholinergic drugs and lesions of nucleus basalis or fimbria-fornix on delayed matching in rats. Psychopharmacology (Berl) 87, 357–363.

Dunnett, S.B., Iversen, S.D., 1981. Learning impairments following selective kainic acid-induced lesions within the neostriatum of rats. Behav. Brain Res. 2, 189–209.

Dunnett, S.B., Nathwani, F., Brasted, P.J., 1999. Medial prefrontal and neostriatal lesions disrupt performance in an operant delayed alternation task in rats. Behav. Brain Res. 106, 13–28.

Eagle, D.M., Humby, T., Dunnett, S.B., Robbins, T.W., 1999. Effects of regional striatal lesions on motor, motivational, and executive aspects of progressive-ratio performance in rats. Behav. Neurosci. 113, 718–731.

Eslamboli, A., Romero-Ramos, M., Burger, C., Bjorklund, T., Muzyczka, N., Mandel, R.J., Baker, H., Ridley, R.M., Kirik, D., 2007. Long-term consequences of human alpha-synuclein overexpression in the primate ventral midbrain. Brain 130, 799–815.

Espa, E., Clemensson, E.K.H., Luk, K.C., Heuer, A., Bjorklund, T., Cenci, M.A., 2019. Seeding of protein aggregation causes cognitive impairment in rat model of cortical synucleinopathy. Mov. Disord. 34, 1699–1710.

Evarts, E.V., Teravainen, H., Calne, D.B., 1981. Reaction time in Parkinson's disease. Brain 104, 167–186.

Fares, M.B., Jagannath, S., Lashuel, H.A., 2021. Reverse engineering Lewy bodies: how far have we come and how far can we go? Nat. Rev. Neurosci. 22, 111–131.

Finkelstein, D.I., Stanic, D., Parish, C.L., Tomas, D., Dickson, K., Horne, M.K., 2000. Axonal sprouting following lesions of the rat substantia nigra. Neuroscience 97, 99–112.
Fujiwara, H., Hasegawa, M., Dohmae, N., Kawashima, A., Masliah, E., Goldberg, M.S., Shen, J., Takio, K., Iwatsubo, T., 2002. alpha-Synuclein is phosphorylated in synucleinopathy lesions. Nat. Cell Biol. 4, 160–164.
Gauntlett-Gilbert, J., Brown, V.J., 1998. Reaction time deficits and Parkinson's disease. Neurosci. Biobehav. Rev. 22, 865–881.
Giasson, B.I., Duda, J.E., Murray, I.V., Chen, Q., Souza, J.M., Hurtig, H.I., Ischiropoulos, H., Trojanowski, J.Q., Lee, V.M., 2000. Oxidative damage linked to neurodegeneration by selective alpha-synuclein nitration in synucleinopathy lesions. Science 290, 985–989.
Gombash, S.E., Manfredsson, F.P., Kemp, C.J., Kuhn, N.C., Fleming, S.M., Egan, A.E., Grant, L.M., Ciucci, M.R., MacKeigan, J.P., Sortwell, C.E., 2013. Morphological and behavioral impact of AAV2/5-mediated overexpression of human wildtype alpha-synuclein in the rat nigrostriatal system. PLoS One 8, e81426.
Gorbatyuk, O.S., Li, S., Sullivan, L.F., Chen, W., Kondrikova, G., Manfredsson, F.P., Mandel, R.J., Muzyczka, N., 2008. The phosphorylation state of Ser-129 in human alpha-synuclein determines neurodegeneration in a rat model of Parkinson disease. Proc. Natl. Acad. Sci. U. S. A. 105, 763–768.
Grealish, S., Mattsson, B., Draxler, P., Bjorklund, A., 2010. Characterisation of behavioural and neurodegenerative changes induced by intranigral 6-hydroxydopamine lesions in a mouse model of Parkinson's disease. Eur. J. Neurosci. 31, 2266–2278.
Gubinelli, F., Cazzolla, G., Negrini, M., Kulacz, I., Mehrdadian, A., Tomasello, G., Venuti, C., Sarauskyte, L., Jacobs, F., Manfredsson, F.P., Davidsson, M., Heuer, A., 2022. Lateralized Deficits after Unilateral AAV-Vector Based Overexpression of Alpha-Synuclein in the Midbrain of Rats on Drug-free Behavioural Tests. Behav Brain Res, 113887.
Hall, H., Jewett, M., Landeck, N., Nilsson, N., Schagerlof, U., Leanza, G., Kirik, D., 2013. Characterization of cognitive deficits in rats overexpressing human alpha-synuclein in the ventral tegmental area and medial septum using recombinant adeno-associated viral vectors. PLoS One 8, e64844.
Hansen, C., Bjorklund, T., Petit, G.H., Lundblad, M., Murmu, R.P., Brundin, P., Li, J.Y., 2013. A novel alpha-synuclein-GFP mouse model displays progressive motor impairment, olfactory dysfunction and accumulation of alpha-synuclein-GFP. Neurobiol. Dis. 56, 145–155.
Harris, J.P., Atkinson, E.A., Lee, A.C., Nithi, K., Fowler, M.S., 2003. Hemispace differences in the visual perception of size in left hemiParkinson's disease. Neuropsychologia 41, 795–807.
Hayashida, K., Oyanagi, S., Mizutani, Y., Yokochi, M., 1993. An early cytoplasmic change before Lewy body maturation: an ultrastructural study of the substantia nigra from an autopsy case of juvenile parkinsonism. Acta Neuropathol. 85, 445–448.
Heuer, A., Dunnett, S.B., 2012. Unilateral 6-OHDA lesions induce lateralised deficits in a 'skinner box' operant choice reaction time task in rats. J. Parkinsons Dis. 2, 309–320.
Heuer, A., Dunnett, S.B., 2013. Characterisation of spatial neglect induced by unilateral 6-OHDA lesions on a choice reaction time task in rats. Behav. Brain Res. 237, 215–222.
Heuer, A., Lelos, M.J., Kelly, C.M., Torres, E.M., Dunnett, S.B., 2013a. Dopamine-rich grafts alleviate deficits in contralateral response space induced by extensive dopamine depletion in rats. Exp. Neurol. 247, 485–495.
Heuer, A., Smith, G.A., Dunnett, S.B., 2013b. Comparison of 6-hydroxydopamine lesions of the substantia nigra and the medial forebrain bundle on a lateralised choice reaction time task in mice. Eur. J. Neurosci. 37, 294–302.
Heuer, A., Vinh, N.N., Dunnett, S.B., 2013c. Behavioural recovery on simple and complex tasks by means of cell replacement therapy in unilateral 6-hydroxydopamine-lesioned mice. Eur. J. Neurosci. 37, 1691–1704.
Hindson, B.J., Ness, K.D., Masquelier, D.A., Belgrader, P., Heredia, N.J., Makarewicz, A. J., Bright, I.J., Lucero, M.Y., Hiddessen, A.L., Legler, T.C., Kitano, T.K., Hodel, M.R., Petersen, J.F., Wyatt, P.W., Steenblock, E.R., Shah, P.H., Bousse, L.J., Troup, C.B., Mellen, J.C., Wittmann, D.K., Erndt, N.G., Cauley, T.H., Koehler, R.T., So, A.P., Dube, S., Rose, K.A., Montesclaros, L., Wang, S., Stumbo, D.P., Hodges, S.P., Romine, S., Milanovich, F.P., White, H.E., Regan, J.F., Karlin-Neumann, G.A., Hindson, C.M., Saxonov, S., Colston, B.W., 2011. High-throughput droplet digital PCR system for absolute quantitation of DNA copy number. Anal. Chem. 83, 8604–8610.
Hsiao, I.T., Weng, Y.H., Hsieh, C.J., Lin, W.Y., Wey, S.P., Kung, M.P., Yen, T.C., Lu, C.S., Lin, K.J., 2014. Correlation of Parkinson disease severity and 18F-DTBZ positron emission tomography. JAMA Neurol. 71, 758–766.
Huang, Y., Halliday, G., 2013. Can we clinically diagnose dementia with Lewy bodies yet? Transl. Neurodegener. 2, 4.
Ip, C.W., Cheong, D., Volkmann, J., 2017. Stereological estimation of dopaminergic neuron number in the mouse substantia nigra using the optical fractionator and standard microscopy equipment, 2017 Sep 1 JoVE J. Vis. Exp. 127, 56103. https://doi.org/10.3791/56103.
Irwin, D.J., Lee, V.M., Trojanowski, J.Q., 2013. Parkinson's disease dementia: convergence of alpha-synuclein, tau and amyloid-beta pathologies. Nat. Rev. Neurosci. 14, 626–636.
Jahanshahi, M., Brown, R.G., Marsden, C.D., 1992. Simple and choice reaction time and the use of advance information for motor preparation in Parkinson's disease. Brain 115 (Pt 2), 539–564.
Jankovic, J., 2008. Parkinson's disease: clinical features and diagnosis. J. Neurol. Neurosurg. Psychiatry 79, 368–376.
Kaasinen, V., Vahlberg, T., 2017. Striatal dopamine in Parkinson disease: a meta-analysis of imaging studies. Ann. Neurol. 82, 873–882.
Kaindlstorfer, C., Garcia, J., Winkler, C., Wenning, G.K., Nikkhah, G., Dobrossy, M.D., 2012. Behavioral and histological analysis of a partial double-lesion model of Parkinson-variant multiple system atrophy. J. Neurosci. Res. 90, 1284–1295.
Kasongo, D.W., de Leo, G., Vicario, N., Leanza, G., Legname, G., 2020. Chronic alpha-synuclein accumulation in rat Hippocampus induces lewy bodies formation and specific cognitive impairments. eNeuro 7.
Kim, S., Cho, S.H., Kim, K.Y., Shin, K.Y., Kim, H.S., Park, C.H., Chang, K.A., Lee, S.H., Cho, D., Suh, Y.H., 2009. Alpha-synuclein induces migration of BV-2 microglial cells by up-regulation of CD44 and MT1-MMP. J. Neurochem. 109, 1483–1496.
Kirik, D., Rosenblad, C., Bjorklund, A., 1998. Characterization of behavioral and neurodegenerative changes following partial lesions of the nigrostriatal dopamine system induced by intrastriatal 6-hydroxydopamine in the rat. Exp. Neurol. 152, 259–277.
Kirik, D., Rosenblad, C., Burger, C., Lundberg, C., Johansen, T.E., Muzyczka, N., Mandel, R.J., Bjorklund, A., 2002. Parkinson-like neurodegeneration induced by targeted overexpression of alpha-synuclein in the nigrostriatal system. J. Neurosci. 22, 2780–2791.
Klein, R.L., Dayton, R.D., Leidenheimer, N.J., Jansen, K., Golde, T.E., Zweig, R.M., 2006. Efficient neuronal gene transfer with AAV8 leads to neurotoxic levels of tau or green fluorescent proteins. Mol. Ther. 13, 517–527.
Klein, R.L., King, M.A., Hamby, M.E., Meyer, E.M., 2002. Dopaminergic cell loss induced by human A30P alpha-synuclein gene transfer to the rat substantia nigra. Hum. Gene Ther. 13, 605–612.
Koprich, J.B., Johnston, T.H., Huot, P., Reyes, M.G., Espinosa, M., Brotchie, J.M., 2011. Progressive neurodegeneration or endogenous compensation in an animal model of Parkinson's disease produced by decreasing doses of alpha-synuclein. PLoS One 6, e17698.
Koprich, J.B., Johnston, T.H., Reyes, G., Omana, V., Brotchie, J.M., 2016. Towards a non-human primate model of alpha-synucleinopathy for development of therapeutics for Parkinson's disease: optimization of AAV1/2 delivery parameters to drive sustained expression of alpha synuclein and dopaminergic degeneration in macaque. PLoS One 11, e0167235.
Koprich, J.B., Johnston, T.H., Reyes, M.G., Sun, X., Brotchie, J.M., 2010. Expression of human A53T alpha-synuclein in the rat substantia nigra using a novel AAV1/2 vector produces a rapidly evolving pathology with protein aggregation, dystrophic neurite architecture and nigrostriatal degeneration with potential to model the pathology of Parkinson's disease. Mol. Neurodegener. 5, 43.
Kordower, J.H., Olanow, C.W., Dodiya, H.B., Chu, Y., Beach, T.G., Adler, C.H., Halliday, G.M., Bartus, R.T., 2013. Disease duration and the integrity of the nigrostriatal system in Parkinson's disease. Brain 136, 2419–2431.
Kurowska, Z., Kordower, J.H., Stoessl, A.J., Burke, R.E., Brundin, P., Yue, Z., Brady, S.T., Milbrandt, J., Trapp, B.D., Sherer, T.B., Medicetty, S., 2016. Is axonal degeneration a key early event in Parkinson's disease? J. Parkinsons Dis. 6, 703–707.
Landeck, N., Buck, K., Kirik, D., 2017. Toxic effects of human and rodent variants of alpha-synuclein in vivo. Eur. J. Neurosci. 45, 536–547.
Laudate, T.M., Neargarder, S., Cronin-Golomb, A., 2013. Line bisection in Parkinson's disease: investigation of contributions of visual field, retinal vision, and scanning patterns to visuospatial function. Behav. Neurosci. 127, 151–163.
Lee, A.C., Harris, J.P., Atkinson, E.A., Fowler, M.S., 2001a. Disruption of estimation of body-scaled aperture width in Hemiparkinson's disease. Neuropsychologia 39, 1097–1104.
Lee, A.C., Harris, J.P., Atkinson, E.A., Fowler, M.S., 2001b. Evidence from a line bisection task for visuospatial neglect in left hemiparkinson's disease. Vis. Res. 41, 2677–2686.
Lelos, M.J., Dowd, E., Dunnett, S.B., 2012. Nigral grafts in animal models of Parkinson's disease. Is recovery beyond motor function possible? Prog. Brain Res. 200, 113–142.
Levin, B.E., Llabre, M.M., Reisman, S., Weiner, W.J., Sanchez-Ramos, J., Singer, C., Brown, M.C., 1991. Visuospatial impairment in Parkinson's disease. Neurology 41, 365–369.
Liberatore, G.T., Finkelstein, D.I., Wong, J.Y., Horne, M.K., Porritt, M.J., Donnan, G.A., Howells, D.W., 1999. Sprouting of dopaminergic axons after striatal injury: confirmation by markers not dependent on dopamine metabolism. Exp. Neurol. 159, 565–573.
Lo Bianco, C., Ridet, J.L., Schneider, B.L., Deglon, N., Aebischer, P., 2002. Alpha -Synucleinopathy and selective dopaminergic neuron loss in a rat lentiviral-based model of Parkinson's disease. Proc. Natl. Acad. Sci. U. S. A. 99, 10813–10818.
Lock, M., Alvira, M.R., Chen, S.J., Wilson, J.M., 2014. Absolute determination of single-stranded and self-complementary adeno-associated viral vector genome titers by droplet digital PCR. Hum. Gene Ther. Methods 25, 115–125.
Lundblad, M., Decressac, M., Mattsson, B., Bjorklund, A., 2012. Impaired neurotransmission caused by overexpression of alpha-synuclein in nigral dopamine neurons. Proc. Natl. Acad. Sci. U. S. A. 109, 3213–3219.
Magen, I., Chesselet, M.F., 2010. Genetic mouse models of Parkinson's disease the state of the art. Prog. Brain Res. 184, 53–87.
Maingay, M., Romero-Ramos, M., Carta, M., Kirik, D., 2006. Ventral tegmental area dopamine neurons are resistant to human mutant alpha-synuclein overexpression. Neurobiol. Dis. 23, 522–532.
Marogianni, C., Sokratous, M., Dardiotis, E., Hadjigeorgiou, G.M., Bogdanos, D., Xiromerisiou, G., 2020. Neurodegeneration and inflammation-an interesting interplay in Parkinson's disease. Int. J. Mol. Sci. 21.
McGeer, P.L., McGeer, E.G., 2004. Inflammation and neurodegeneration in Parkinson's disease. Park. Relat. Disord. 10 (Suppl. 1), S3–S7.
Montoya, C.P., Astell, S., Dunnett, S.B., 1990. Effects of nigral and striatal grafts on skilled forelimb use in the rat. Prog. Brain Res. 82, 459–466.

Musacchio, T., Rebenstorff, M., Fluri, F., Brotchie, J.M., Volkmann, J., Koprich, J.B., Ip, C.W., 2017. Subthalamic nucleus deep brain stimulation is neuroprotective in the A53T alpha-synuclein Parkinson's disease rat model. Ann. Neurol. 81, 825–836.
Negrini, M., Tomasello, G., Davidsson, M., Fenyi, A., Adant, C., Hauser, S., Espa, E., Gubinelli, F., Manfredsson, F.P., Melki, R., Heuer, A., 2022. Sequential or simultaneous injection of preformed fibrils and AAV overexpression of alpha-synuclein are equipotent in producing relevant pathology and behavioral deficits. J. Parkinsons Dis.
Negrini, M., Wang, G., Heuer, A., Bjorklund, T., Davidsson, M., 2020. AAV production everywhere: a simple, fast, and reliable protocol for in-house AAV vector production based on chloroform extraction. Curr Protoc Neurosci 93, e103.
Obeso, J.A., Stamelou, M., Goetz, C.G., Poewe, W., Lang, A.E., Weintraub, D., Burn, D., Halliday, G.M., Bezard, E., Przedborski, S., Lehericy, S., Brooks, D.J., Rothwell, J.C., Hallett, M., DeLong, M.R., Marras, C., Tanner, C.M., Ross, G.W., Langston, J.W., Klein, C., Bonifati, V., Jankovic, J., Lozano, A.M., Deuschl, G., Bergman, H., Tolosa, E., Rodriguez-Violante, M., Fahn, S., Postuma, R.B., Berg, D., Marek, K., Standaert, D.G., Surmeier, D.J., Olanow, C.W., Kordower, J.H., Calabresi, P., Schapira, A.H.V., Stoessl, A.J., 2017. Past, present, and future of Parkinson's disease: a special essay on the 200th Anniversary of the Shaking Palsy. Mov. Disord. 32, 1264–1310.
Oliveras-Salva, M., Van der Perren, A., Casadei, N., Stroobants, S., Nuber, S., D'Hooge, R., Van den Haute, C., Baekelandt, V., 2013. rAAV2/7 vector-mediated overexpression of alpha-synuclein in mouse substantia nigra induces protein aggregation and progressive dose-dependent neurodegeneration. Mol. Neurodegener. 8, 44.
Olsson, M., Nikkhah, G., Bentlage, C., Bjorklund, A., 1995. Forelimb akinesia in the rat Parkinson model: differential effects of dopamine agonists and nigral transplants as assessed by a new stepping test. J. Neurosci. 15, 3863–3875.
Onn, S.P., Berger, T.W., Stricker, E.M., Zigmond, M.J., 1986. Effects of intraventricular 6-hydroxydopamine on the dopaminergic innervation of striatum: histochemical and neurochemical analysis. Brain Res. 376, 8–19.
Ormo, M., Cubitt, A.B., Kallio, K., Gross, L.A., Tsien, R.Y., Remington, S.J., 1996. Crystal structure of the Aequorea victoria green fluorescent protein. Science 273, 1392–1395.
Phan, J.A., Stokholm, K., Zareba-Paslawska, J., Jakobsen, S., Vang, K., Gjedde, A., Landau, A.M., Romero-Ramos, M., 2017. Early synaptic dysfunction induced by alpha-synuclein in a rat model of Parkinson's disease. Sci. Rep. 7, 6363.
Phani, S., Loike, J.D., Przedborski, S., 2012. Neurodegeneration and inflammation in Parkinson's disease. Park. Relat. Disord. 18 (Suppl. 1), S207–S209.
Phillips, J.M., Brown, V.J., 1999. Reaction time performance following unilateral striatal dopamine depletion and lesions of the subthalamic nucleus in the rat. Eur. J. Neurosci. 11, 1003–1010.
Quintino, L., Gubinelli, F., Sarauskyte, L., Arvidsson, E., Davidsson, M., Lundberg, C., Heuer, A., 2022. Automated quantification of neuronal swellings in a preclinical rodent model of Parkinson's disease detects region-specific changes in pathology. J. Neurosci. Methods 378, 109640.
Rea, L.M., Parker, R.A., 2014. Designing and Conducting Survey Research: A Comprehensive Guide.
Reading, P.J., Dunnett, S.B., Robbins, T.W., 1991. Dissociable roles of the ventral, medial and lateral striatum on the acquisition and performance of a complex visual stimulus-response habit. Behav. Brain Res. 45, 147–161.
Ren, S., He, K., Girshick, R., Sun, J., 2017. Faster R-CNN: towards real-time object detection with region proposal networks. IEEE Trans. Pattern Anal. Mach. Intell. 39, 1137–1149.
Robbins, T.W., Roberts, D.C., Koob, G.F., 1983. Effects of d-amphetamine and apomorphine upon operant behavior and schedule-induced licking in rats with 6-hydroxydopamine-induced lesions of the nucleus accumbens. J. Pharmacol. Exp. Therapeut. 224, 662–673.
Robinson, T.E., Whishaw, I.Q., 1988. Normalization of extracellular dopamine in striatum following recovery from a partial unilateral 6-OHDA lesion of the substantia nigra: a microdialysis study in freely moving rats. Brain Res. 450, 209–224.
Rogers, M.W., Chan, C.W., 1988. Motor planning is impaired in Parkinson's disease. Brain Res. 438, 271–276.
Sanchez-Guajardo, V., Febbraro, F., Kirik, D., Romero-Ramos, M., 2010. Microglia acquire distinct activation profiles depending on the degree of alpha-synuclein neuropathology in a rAAV based model of Parkinson's disease. PLoS One 5, e8784.
Sandoval, I.M., Kuhn, N.M., Manfredsson, F.P., 2019. Multimodal production of adeno-associated virus. Methods Mol. Biol. 1937, 101–124.
Schallert, T., Fleming, S.M., Leasure, J.L., Tillerson, J.L., Bland, S.T., 2000. CNS plasticity and assessment of forelimb sensorimotor outcome in unilateral rat models of stroke, cortical ablation, parkinsonism and spinal cord injury. Neuropharmacology 39, 777–787.
Spillantini, M.G., Crowther, R.A., Jakes, R., Cairns, N.J., Lantos, P.L., Goedert, M., 1998a. Filamentous alpha-synuclein inclusions link multiple system atrophy with Parkinson's disease and dementia with Lewy bodies. Neurosci. Lett. 251, 205–208.
Spillantini, M.G., Crowther, R.A., Jakes, R., Hasegawa, M., Goedert, M., 1998b. alpha-Synuclein in filamentous inclusions of Lewy bodies from Parkinson's disease and dementia with lewy bodies. Proc. Natl. Acad. Sci. U. S. A. 95, 6469–6473.
Spillantini, M.G., Schmidt, M.L., Lee, V.M., Trojanowski, J.Q., Jakes, R., Goedert, M., 1997. Alpha-synuclein in lewy bodies. Nature 388, 839–840.
Su, X., Federoff, H.J., Maguire-Zeiss, K.A., 2009. Mutant alpha-synuclein overexpression mediates early proinflammatory activity. Neurotox. Res. 16, 238–254.
Su, X., Maguire-Zeiss, K.A., Giuliano, R., Prifti, L., Venkatesh, K., Federoff, H.J., 2008. Synuclein activates microglia in a model of Parkinson's disease. Neurobiol. Aging 29, 1690–1701.
Tagliaferro, P., Burke, R.E., 2016. Retrograde axonal degeneration in Parkinson disease. J. Parkinsons Dis. 6, 1–15.
Thakur, P., Breger, L.S., Lundblad, M., Wan, O.W., Mattsson, B., Luk, K.C., Lee, V.M.Y., Trojanowski, J.Q., Bjorklund, A., 2017. Modeling Parkinson's disease pathology by combination of fibril seeds and alpha-synuclein overexpression in the rat brain. Proc. Natl. Acad. Sci. U. S. A. 114, E8284–E8293.
Theodore, S., Cao, S., McLean, P.J., Standaert, D.G., 2008. Targeted overexpression of human alpha-synuclein triggers microglial activation and an adaptive immune response in a mouse model of Parkinson disease. J. Neuropathol. Exp. Neurol. 67, 1149–1158.
Torres, E.M., Lane, E.L., Heuer, A., Smith, G.A., Murphy, E., Dunnett, S.B., 2011. Increased efficacy of the 6-hydroxydopamine lesion of the median forebrain bundle in small rats, by modification of the stereotaxic coordinates. J. Neurosci. Methods 200, 29–35.
Truong, L., Allbutt, H., Kassiou, M., Henderson, J.M., 2006. Developing a preclinical model of Parkinson's disease: a study of behaviour in rats with graded 6-OHDA lesions. Behav. Brain Res. 169, 1–9.
Ungerstedt, U., 1968. 6-Hydroxy-dopamine induced degeneration of central monoamine neurons. Eur. J. Pharmacol. 5, 107–110.
Van der Perren, A., Toelen, J., Casteels, C., Macchi, F., Van Rompuy, A.S., Sarre, S., Casadei, N., Nuber, S., Himmelreich, U., Osorio Garcia, M.I., Michotte, Y., D'Hooge, R., Bormans, G., Van Laere, K., Gijsbers, R., Van den Haute, C., Debyser, Z., Baekelandt, V., 2015. Longitudinal follow-up and characterization of a robust rat model for Parkinson's disease based on overexpression of alpha-synuclein with adeno-associated viral vectors. Neurobiol. Aging 36, 1543–1558.
Villardita, C., Smirni, P., Zappala, G., 1983. Visual neglect in Parkinson's disease. Arch. Neurol. 40, 737–739.
Wakabayashi, K., Tanji, K., Mori, F., Takahashi, H., 2007. The Lewy body in Parkinson's disease: molecules implicated in the formation and degradation of alpha-synuclein aggregates. Neuropathology 27, 494–506.
Wakabayashi, K., Tanji, K., Odagiri, S., Miki, Y., Mori, F., Takahashi, H., 2013. The Lewy body in Parkinson's disease and related neurodegenerative disorders. Mol. Neurobiol. 47, 495–508.
Wise, R.A., 2004. Dopamine, learning and motivation. Nat. Rev. Neurosci. 5, 483–494.
Yamada, M., Iwatsubo, T., Mizuno, Y., Mochizuki, H., 2004. Overexpression of alpha-synuclein in rat substantia nigra results in loss of dopaminergic neurons, phosphorylation of alpha-synuclein and activation of caspase-9: resemblance to pathogenetic changes in Parkinson's disease. J. Neurochem. 91, 451–461.
Zhou, L., Miller, B.L., McDaniel, C.H., Kelly, L., Kim, O.J., Miller, C.A., 1998. Frontotemporal dementia: neuropil spheroids and presynaptic terminal degeneration. Ann. Neurol. 44, 99–109.